Engineering Structures 272 (2022) 114988

Contents lists available at ScienceDirect

Engineering Structures

journal homepage: www.elsevier.com/locate/engstruct

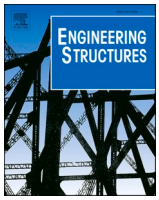

Fibre-Based modelling for predicting the progressive collapse of cylindrical shells under combined axial compression and bending moment

Shen Li [a,*], Do Kyun Kim [b,c,*], Qing Quan Liang [d,*]

[a] Department of Naval Architecture, Ocean and Marine Engineering, University of Strathclyde, Glasgow, United Kingdom
[b] Department of Naval Architecture and Ocean Engineering, Seoul National University, Seoul, Republic of Korea
[c] Institute of Engineering Research & Research Institute of Marine Systems Engineering, Seoul National University, Seoul, Republic of Korea
[d] College of Engineering and Science, Victoria University, Melbourne, Australia

ARTICLE INFO

Keywords:
Cylindrical shell
Buckling
Ultimate strength
Collapse
Fibre-based modelling

ABSTRACT

Cylindrical shell is a fundamental building block of many engineering structures. They are usually designed to be the primary load-carrying components to withstand different combinations of environmental loads. This paper presents a fibre-based approach to modelling the progressive collapse of cylindrical shells under combined axial compression and bending moment. In this method, the progressive collapse behaviour of cylindrical shells is incrementally evaluated by accounting for the local response of each fibre element. This approach offers a computationally efficient and robust scheme to compute the ultimate strength of cylindrical shells. Moreover, it enables the modelling of load-shedding between the buckled and intact shell elements on the compressive side, and the yielding failure on the tensile side, which appears to be ignored in existing design codes. Analyses are performed on cylindrical shells with a wide range of design parameters. Validation using the finite element method demonstrates a reasonably well performance of the proposed fibre-based modelling technique.

1. Introduction

Cylindrical shells are commonly used as structural elements in different engineering fields, such as offshore platforms supporting foundations and submarine pressure hulls in the maritime sector. They usually are designed as the principal load-carrying components to withstand axial compression, bending moment and external pressure as the resultants of the wind, wave and current actions. A rational evaluation of the structural performance of these critical structural elements is crucial for the integrity and safe operation of infrastructure. Limit state design is the contemporary integrity and safety assessment philosophy for marine structures [1]. Four types of limit state are typically assessed, i.e., serviceability limit state, accidental limit state, fatigue limit state and ultimate limit state. Whilst all criteria are important, the ultimate limit state is usually the basis for determining the principal structural scantling in an initial stage.

In terms of the ultimate limit state assessment of cylindrical shells, there are several design guidelines issued by different certification authorities, e.g., DNV [2], ABS [3], API, [4] and Eurocode [5], which include various analytical formulae to predict the ultimate strength of cylindrical shells. These formulations all appear to be an adaptation of the classical buckling strength formula, with different correction factors to account for the discrepancy between the theoretical estimation and physical experimental measurement. However, these analytical formulae only provide the estimation of the ultimate capacity of cylindrical shells but are unable to predict the load–displacement relation over the entire course of collapse, i.e., progressive collapse behaviour. Understanding the entire progressive collapse behaviour could have several benefits: 1) as the local failure progressively occurs before the ultimate collapse, the prediction of the entire progressive collapse behaviour can inform the structural designers of the most critical structural component; 2) the post-collapse unloading reveals the failure tolerance of the structures. If the cylindrical shell is part of a structural assembly, rapid post-collapse unloading would accelerate the collapse of the entire assembly.

Furthermore, most of these code-based approaches predict the collapse strength under axial compression and bending moment using the same formulation. This is likely based on the assumption that the overall structural collapse due to the bending moment would occur when the furthest edge from the neutral axis reaches the compressive limit. This may be overly conservative as the cylindrical shell should generally be able to carry more external loads because of the load-

* Corresponding authors.
E-mail addresses: shen.li@strath.ac.uk (S. Li), do.kim@snu.ac.kr (D.K. Kim), qing.liang@vu.edu.au (Q.Q. Liang).

https://doi.org/10.1016/j.engstruct.2022.114988
Received 11 March 2022; Received in revised form 14 September 2022; Accepted 18 September 2022
Available online 29 September 2022

shedding between the buckled and intact elements. Thus, the critical buckling strength under pure bending can be appreciably larger than that under pure compression [6].

To account for the above considerations, the application of the nonlinear finite element method (NLFEM) considering both geometric and material nonlinearities may be the best solution. There are many studies on this topic performed by the nonlinear finite element method. Kim and Kim [7] conducted a parametric numerical study on unstiffened cylindrical shells under axial compression. Cerik [8] reported a numerical investigation on the residual strength of ring-stiffened and orthogonally stiffened damaged cylindrical shells under axial compression. Li and Kim [9] presented a numerical analysis of unstiffened cylindrical shells under axial compression. In particular, they investigated the sensitivity to initial geometric imperfection and compared the numerical prediction with design code estimations. Nevertheless, nonlinear finite element analysis requires dedicated modelling expertise, including geometry modelling, meshing [58], application of geometric imperfection and calibration of numerical parameters. Furthermore, the required computational time is still a significant drawback, especially if many analyses need to be performed for different design alternatives, such as that in reliability analysis and structural optimisation.

In this regard, a fibre-based modelling approach is proposed in this paper, which can provide more accurate ultimate strength prediction for cylindrical shells by considering load-shedding and remaining computationally efficient. The fibre-based approach is a displacement-driven numerical technique, which predicts the global collapse behaviour of cylindrical shells by evaluating the local fibre response due to the global load effect, e.g., axial compression induced by bending. In the remainder of this paper, a literature review of the fibre-based method is given in Section 2. The proposed fibre-based formulation is described in Section 3. Comparison with the nonlinear finite element method is presented in Section 4 for a parametric range of structural dimensions and load combinations. The effects of various parameters on the behaviour of cylindrical shells are examined in Section 5. Conclusions and the recommended future works are summarised in Section 6.

2. Literature review

The fibre-based modelling has been extensively used for analysing the behaviour of concrete-filled and reinforced concrete columns in civil engineering. Compared with the conventional finite element method, the fibre-based approach saves the model development and computational time significantly. It has been proved to be an accurate numerical method for modelling the inelastic behaviour of composite columns [10–11]. Liang [12] developed a new numerical method based on fibre-based modelling technology for predicting the ultimate strength of double-skin concrete-filled steel tubular columns under axial compression. Liang [13] presented a mathematical model for simulating the high strength circular double-skin concrete-filled steel tubular slender columns under eccentric loading. Ahmed et al. [14] analysed the preload effects using fibre-based approach on the performance of axially and eccentrically loaded square concrete-filled double steel tubular slender columns. Rizwan et al. [15] introduced a fibre-based model for rectangular double-skin concrete-filled steel tubular short columns considering local buckling. Numerical analysis on rectangular double-skin concrete-filled steel tubular slender columns was presented by Rizwan et al. [16] using a fibre-based model considering local and global interaction buckling. Likewise, the effect of buckling interaction was investigated by Phan et al. [17] using fibre-based methodology for uniaxially compressed square ultra-high-strength concrete-filled steel tubular slender beam-columns. Phan et al. [18] developed a fibre-based model for determining the structural behaviour of eccentrically loaded circular double-skin steel tubular slender beam-columns filled with ultra-high-strength concrete. Ahmed et al. [19] studied the circular double-skin concrete-filled stainless-carbon steel tubular columns under axial load and bending using a fibre-based modelling approach. Al-Jelawy and Mackie [20] developed a three-dimensional fibre-based model for precast and cast-in-place reinforced concrete columns. Aldabagh et al. [21] proposed a simplified predictive expression for predicting the drift limit states of reinforced concrete circular columns based on the numerical results by utilising the fibre-based model.

In the maritime sector, this concept was applied by Dow and Smith [22] to develop the computer code FABSTRAN for predicting the progressive collapse and ultimate strength of beam-columns under axial compression, in which the stiffener of a stiffened plated structures was discretised into a set of fibres. A more common generalisation or variation of the fibre-based concept in the marine field is the Smith-type progressive collapse method or referred to as the incremental/iterative method in classification society rule [23]. It was initially developed in the 1970s to predict the ultimate strength of ship hull girders under vertical bending [24]. The progressive collapse approach was then formalised and validated for the first time by Dow et al. [25] using small-scaled box girder tests. The advancement to this method has continued in recent years. Benson et al. [26] extended the original approach by removing the interframe buckling assumption. This was driven by an adapted orthotropic plate theory developed in [27] to derive the load-shortening curves of the entire grillage rather than individual plate-stiffener combination (i.e., beam-column). An extended formulation was introduced by Syrigou et al. [28] to consider the effect of torsion. Li et al. [29–30] proposed a progressive collapse method to evaluate the strength degradation of ship hull girders due to extreme cyclic loads. Tatsumi et al. [31] extended the Smith method to account for the effect caused by the local bending of the double bottom of ships. Aside from various extended formulations, the Smith-type progressive collapse has been widely applied to evaluate the residual strength of damaged ship structures [32–33] and probabilistic assessment of ship structural strength [34–35].

A similar methodology to the Smith-type progressive collapse method was the Intelligent Supersize Finite Element Method (ISFEM), which was developed to resolve the high computational requirement of the conventional finite element method (FEM) [36]. The pioneering development of this approach, which was named the Idealised Structural Unit Method (ISUM), was reported by Ueda and Rashed [37]. In contrast to the conventional FEM, the ISFEM is said to be intelligent because the highly nonlinear behaviour of the large elements is educated or formulated in advance, generating a high level of intelligence in terms of judging the failure status and modes of such a large element. The ISFEM overcomes the high computational requirement in conventional FEM but still retains the versatility to analyse the nonlinear inelastic large deflection behaviours of different steel and aluminium structures, such as ship hulls, bridges, and cranes [38–40].

3. Methodology

3.1. Global response formulation

A fibre-based approach is developed herein as an efficient computational method for simulating the progressive collapse of cylindrical shells under combined compression and bending moment. The following assumptions are made for the development of fibre-based approach:

1. The behaviour of each fibre is independent and can be represented by a load–shortening curve characterising its stress/strain response to in-plane load.
2. The resultant strain at each fibre of the cross section follows a linear distribution through the section depth for a given bending moment increment during the entire progressive collapse process.
3. The Euler column-type buckling is negligible, and the buckling failure occurs in an interframe manner, meaning that the failure will primarily be induced by buckling in localised region, i.e., shell

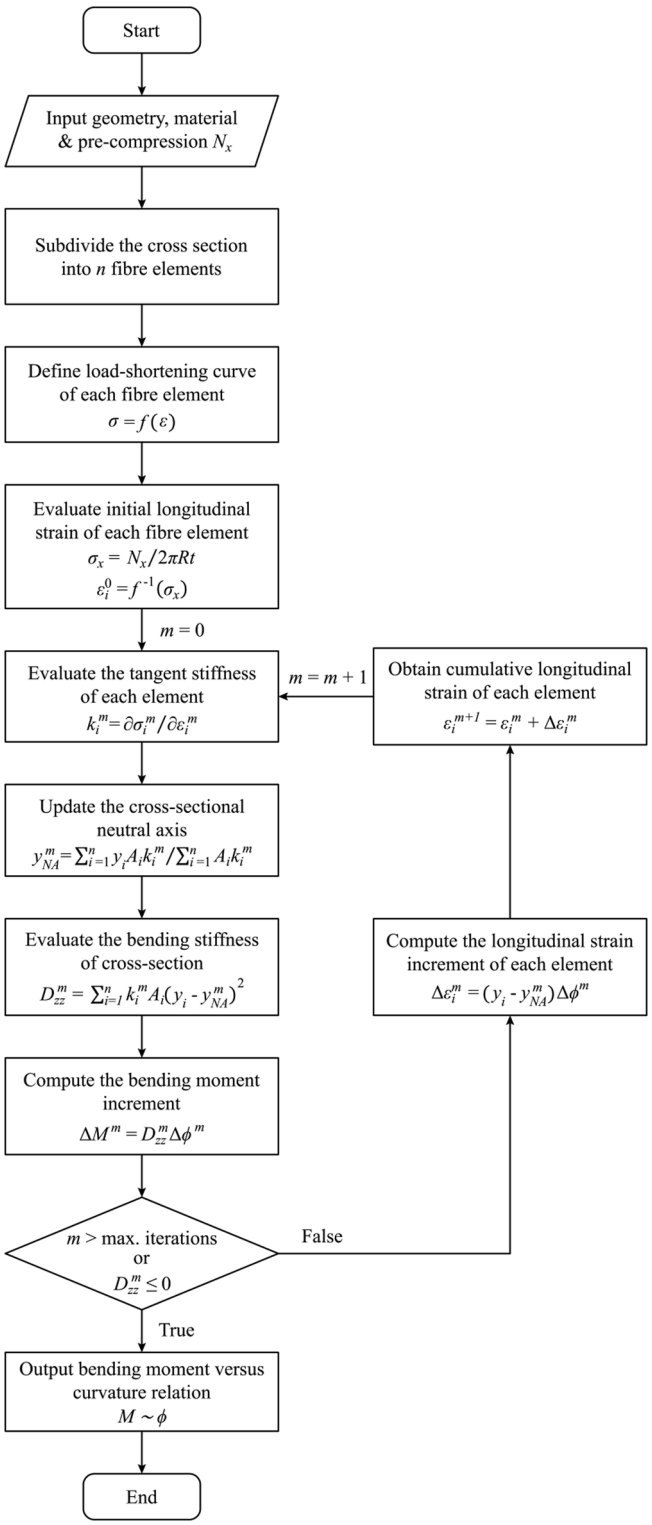

Fig. 1. Flowchart of the proposed fibre-based modelling procedure.

buckling in the case of unstiffened column, or bay buckling only in the case of ring-stiffened columns.

The first assumption generally holds when each fibre within the cylindrical shell is primarily subjected to axial loading, i.e., either directly by axial compression or induced by global bending. The second assumption should be reasonable before the ultimate collapse occurs. The third assumption is valid for cylindrical columns with a small length-to-radius ratio or cylindrical shells with stocky transverse stiffening.

The proposed fibre-based modelling consists of global response formulation and local response formulation. The formulation to simulate the global response of cylindrical shells under combined axial compression and bending moment is given in Equation (1) to Equation (5).

$$\Delta M^m = D_{zz}^m \Delta\phi^m \tag{1}$$

$$D_{zz}^m = \sum_{i=1}^{n} k_i^m A_i \left(y_i - y_{NA}^m\right)^2 \tag{2}$$

$$k_i^m = \partial\sigma_i^m / \partial\varepsilon_i^m \tag{3}$$

$$y_{NA}^m = \sum\nolimits_1^i y_i A_i k_i^m / \sum\nolimits_1^i A_i k_i^m \tag{4}$$

$$\Delta\varepsilon_i^m = \left(y_i - y_{NA}^m\right)\Delta\phi^m \tag{5}$$

$$M^{m+1} = M^m + \Delta M^m \tag{6}$$

$$\phi^{m+1} = \phi^m + \Delta\phi^m \tag{7}$$

$$\varepsilon_i^{m+1} = \varepsilon_i^m + \Delta\varepsilon_i^m \tag{8}$$

where ΔM^m is the bending moment increment at incremental step m, $\Delta\phi^m$ is the curvature increment at incremental step m, D_{zz}^m is the nonlinear bending stiffness at incremental step m, k_i^m is the tangent stiffness of structural element i at incremental step m, y_{NA}^m is the vertical coordinate of the instantaneous cross-sectional neutral axis of the cylindrical shell, y_i is the vertical coordinate of the neutral axis of structural element i, A_i is the cross-sectional area of the structural element i, $\Delta\varepsilon_i^m$ is the strain increment of structural element i at incremental step m, σ_i^m is the instantaneous longitudinal stress of structural element i at incremental step m, ε_i^m is the instantaneous longitudinal strain of structural element i at incremental step m.

The computational procedure may be elucidated with reference to the flowchart shown in Fig. 1. Once the geometry, material property and pre-loaded compression are defined, the cross section of the cylindrical shell is first subdivided into a set of small fibres. Linear and uniform distributions of the longitudinal strain of fibre element induced by bending moment and axial compression respectively are assumed (Fig. 2). Each fibre element is assigned with a load-shortening curve to characterise its stress response to longitudinal straining induced by axial compression, bending moment and their combinations. Assuming that the cross section remains plane during the progressive collapse, cross-sectional curvature is applied incrementally about the instantaneous neutral axis. The incremental bending moment is computed with the applied curvature increment and cross-sectional bending stiffness (i.e., Equation (1)). The cross-sectional bending stiffness is evaluated by the elemental tangent stiffness. (i.e., Equation (2)). The element tangent stiffness is estimated as the derivative of the load-shortening curve at the instantaneous elemental strain (i.e., Equation (3)). In terms of pure bending, the initial elemental strain is specified as null. Conversely, in the case of combined compression and bending, the initial elemental strain is the resultant strain due to the pre-loaded compression. The position of the instantaneous neutral axis is updated at each incremental step through an adapted first moment of area of the cross section, which accounts for the loss of load-carrying effectiveness of each element (i.e., Equation (4)). The incremental longitudinal strain of each element is evaluated by Equation (5), which drives the update of elemental tangent stiffness for incremental calculation. Cumulative values of curvature, bending moment and elemental strain are obtained by Equations (6) to (8). They are output when the termination criterion is met, for instance, when the bending stiffness becomes negative or the post-collapse strength is reduced to half of the ultimate strength.

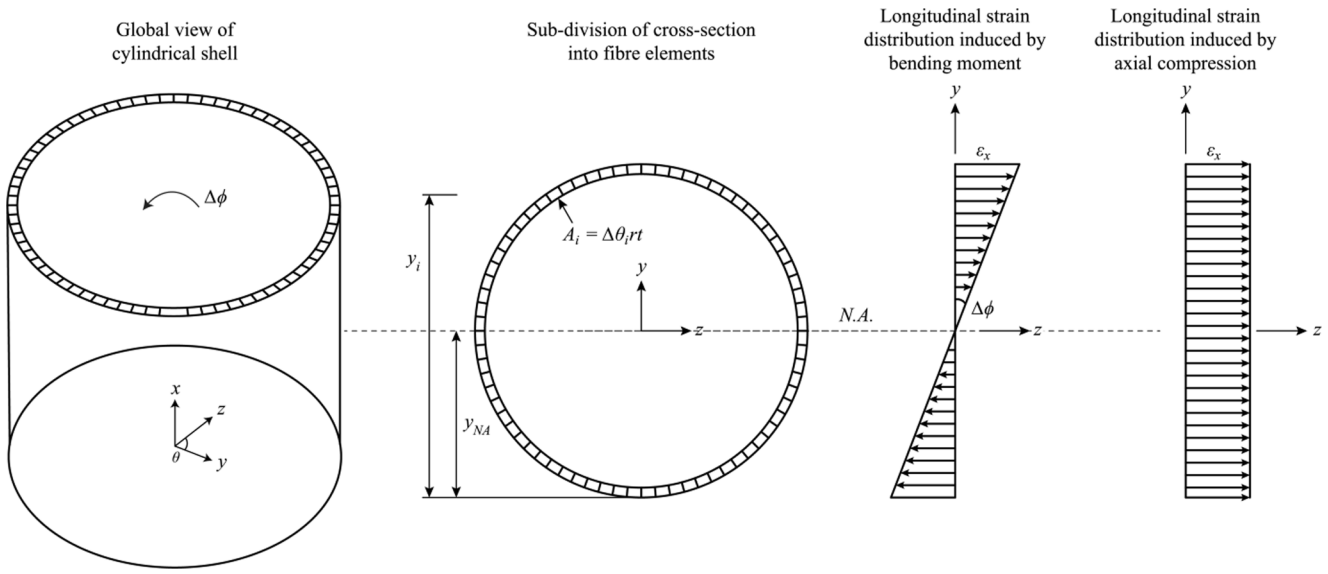

Fig. 2. Fibre-based modelling of cylindrical shell under bending moment.

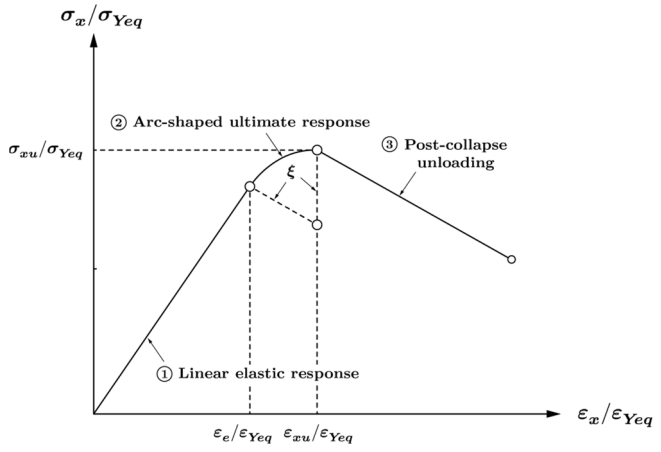

Fig. 3. Schematics of local response formulation.

3.2. Local response formulation

Due to the global bending, each fibre element undergoes longitudinal in-plane loading, i.e. tension or compression. Elastic-perfectly plastic behaviour would be a reasonable approximation for the tensile response. To simulate the local response of fibre element under compressive longitudinal straining, i.e., compressive load-shortening curve, an efficient semi-empirical method is applied in this paper. Whilst this method was initially derived for stiffened plated structures under longitudinal compression [41], it is a generic formulation that can be applied to different structural stability and buckling collapse problems. In this approach, the load-shortening response of cylindrical shell under longitudinal loads is idealised as three distinct parts: initial elastic response, nonlinear response from the onset of buckling till attaining ultimate strength, and post-collapse unloading. As depicted in Fig. 3, the initial elastic response is governed by the initial stiffness. An arc-shaped approximation is employed for the nonlinear response from the onset of buckling till attaining ultimate strength, in which the tangent stiffness decreases from that specified for the initial elastic state to null at the ultimate limit state. As for the post-collapse response, a linear response is assumed in this paper for simplicity. Future works may consider a more realistic exponential post-collapse unloading behaviour.

The expressions of the proposed method for simulating compressive load-shortening response are given as follows:

$\frac{\sigma_x}{\sigma_Y} = \overline{E}_{To}\frac{\varepsilon_x}{\varepsilon_Y}$ for $\frac{\varepsilon_x}{\varepsilon_Y} \le \frac{\varepsilon_{xe}}{\varepsilon_Y}$ (9).

$$\frac{\sigma_x}{\sigma_Y} = \frac{\sigma_{xu}}{\sigma_Y} - \xi + \xi cos\left[-tan^{-1}(\overline{E}_T)\right] \text{ for } \frac{\varepsilon_{xe}}{\varepsilon_Y} < \frac{\varepsilon_x}{\varepsilon_Y} \le \frac{\varepsilon_{xu}}{\varepsilon_Y} \tag{10}$$

$$\frac{\sigma_x}{\sigma_Y} = \frac{\sigma_{xu}}{\sigma_Y} + E_{Tp}\left(\frac{\varepsilon_x}{\varepsilon_Y} - \frac{\varepsilon_{xu}}{\varepsilon_Y}\right) \text{ for } \frac{\varepsilon_x}{\varepsilon_Y} > \frac{\varepsilon_{xu}}{\varepsilon_Y} \tag{11}$$

where.

$$\xi = \frac{cos[tan^{-1}(\overline{E}_{To})](\overline{E}_{To}\varepsilon_{xu}/\varepsilon_Y - \sigma_{xu}/\sigma_Y)}{1 - cos[tan^{-1}(\overline{E}_{To})]}$$

$$\frac{\varepsilon_{xe}}{\varepsilon_Y} = \frac{\varepsilon_{xu}}{\varepsilon_Y} + \xi sin\left[-tan^{-1}(\overline{E}_{To})\right]$$

The above formulation only provides a general framework to predict the compressive load-shortening response. The initial stiffness ($\overline{E}_{To}$), post-collapse stiffness (E_{Tp}), ultimate strain ($\varepsilon_{xu}/\varepsilon_Y$) and ultimate compressive strength (σ_{xu}/σ_Y) are prescribed values which can be determined using any approach based on different model assumptions,

Table 1
Principal particulars of cylindrical shell models.

No.	L/R	R/t	L [mm]	R [mm]	t [mm]	σ_Y [MPa]	E [GPa]
1	0.4	50	2000	5000	100	355	207
2	0.4	100	2000	5000	50	355	207
3	0.4	200	2000	5000	25	355	207
4	0.4	400	2000	5000	12.5	355	207
5	0.6	50	3000	5000	100	355	207
6	0.6	100	3000	5000	50	355	207
7	0.6	200	3000	5000	25	355	207
8	0.6	400	3000	5000	12.5	355	207
9	0.8	50	4000	5000	100	355	207
10	0.8	100	4000	5000	50	355	207
11	0.8	200	4000	5000	25	355	207
12	0.8	400	4000	5000	12.5	355	207
13	1.0	50	5000	5000	100	355	207
14	1.0	100	5000	5000	50	355	207
15	1.0	200	5000	5000	25	355	207
16	1.0	400	5000	5000	12.5	355	207
17	1.2	50	6000	5000	100	355	207
18	1.2	100	6000	5000	50	355	207
19	1.2	200	6000	5000	25	355	207
20	1.2	400	6000	5000	12.5	355	207

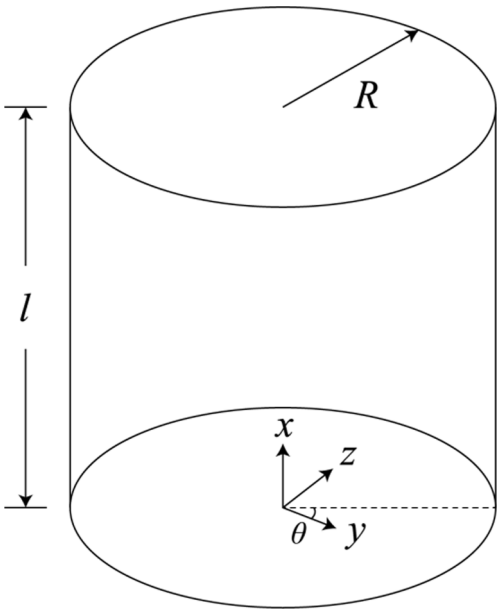

Fig. 4. Coordinate system of cylindrical shell.

so that specific response characteristics and secondary load effects (i.e., external pressure and shear etc.) can be incorporated.

4. Validation

4.1. Test matrix

A total of 20 cylindrical shell models have been compared, with the following parameters systematically varied:

- Length to radius ratio: L/R = 1.2, 1.0, 0.8, 0.6, 0.4
- Radius to thickness ratio: R/t = 50, 100, 200, 400

The radius of all models kept the same as 5000 mm, and the other dimensions (length and thickness) were changed according to the non-dimensional parameters. The material yield stress (σ_Y) and elastic modulus (E) were 355 MPa and 207GPa, respectively. Table 1 gives a summary of all models for comparison. As shown in [8,42–45], the radius-to-thickness ratio of cylindrical shell in maritime sector is typically in the range of 50 to 300. The length-to-radius ratio, considering bay length between transverse supports in the case of ring-stiffened cylinder, is normally in the range of 0.4 to 0.6. Hence, the test matrix in this work covers the common configuration of cylindrical shell structures used in marine infrastructures. Nevertheless, it is acknowledged that the applicability of the proposed should be limited to the present test matrix until a more extended validation exercise is completed.

For each case study model, the following load cases (5 scenarios) were considered:

- Pure compression
- Pure bending
- Combined bending and axial compression with $N_x/N_{xu} = 0.25$
- Combined bending and axial compression with $N_x/N_{xu} = 0.50$
- Combined bending and axial compression with $N_x/N_{xu} = 0.75$

To sum up, $20 \times 5 = 100$ test cases in total have been completed.

4.2. Finite element modelling

For validation purposes, equivalent nonlinear finite element analysis

Table 2
First-order buckling modes predicted by linear eigenvalue analysis.

No.	L/R [-]	R/t [-]	m	n
1	0.4	50	1	6
2	0.4	100	2	6
3	0.4	200	3	7
4	0.4	400	4	10
5	0.6	50	2	5
6	0.6	100	3	6
7	0.6	200	5	0
8	0.6	400	7	0
9	0.8	50	2	6
10	0.8	100	3	9
11	0.8	200	6	6
12	0.8	400	9	0
13	1.0	50	3	6
14	1.0	100	5	6
15	1.0	200	8	0
16	1.0	400	11	0
17	1.2	50	3	6
18	1.2	100	4	9
19	1.2	200	9	6
20	1.2	400	13	0

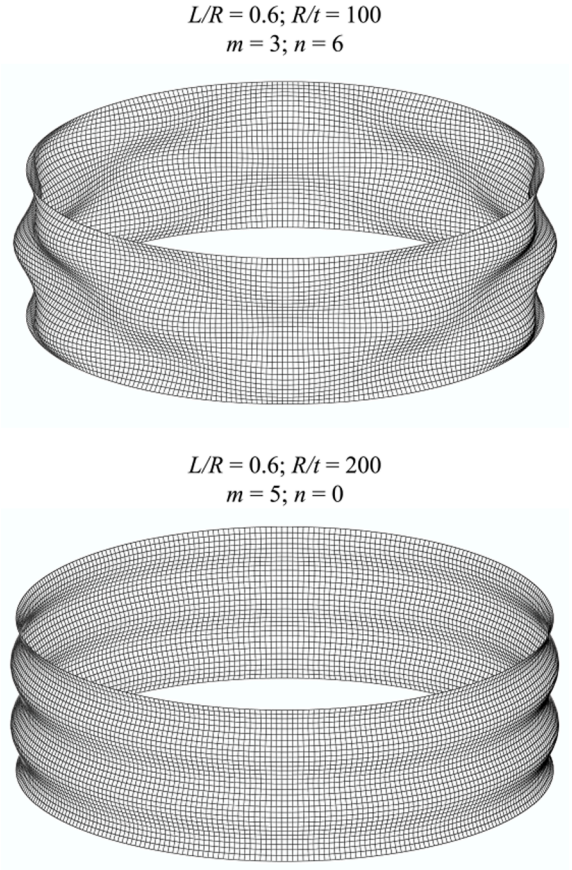

Fig. 5. Example illustration of first order eigen modes: non-rotational-symmetric versus rotational-symmetric (Magnification factor = 50).

was performed. Four-node shell element was employed for the finite element modelling. Geometric imperfection was incorporated, in which the imperfection shape is described as follows:

$$w(x,\theta) = w_{max} sin\left(\frac{m\pi x}{l}\right) sin(n\theta) \tag{12}$$

where a cylindrical coordinate is adopted. As depicted in Fig. 4, any position within the cylindrical shell is expressed by combining longitudinal coordinate (x) and angular coordinate (θ). w_{max} is the maximum

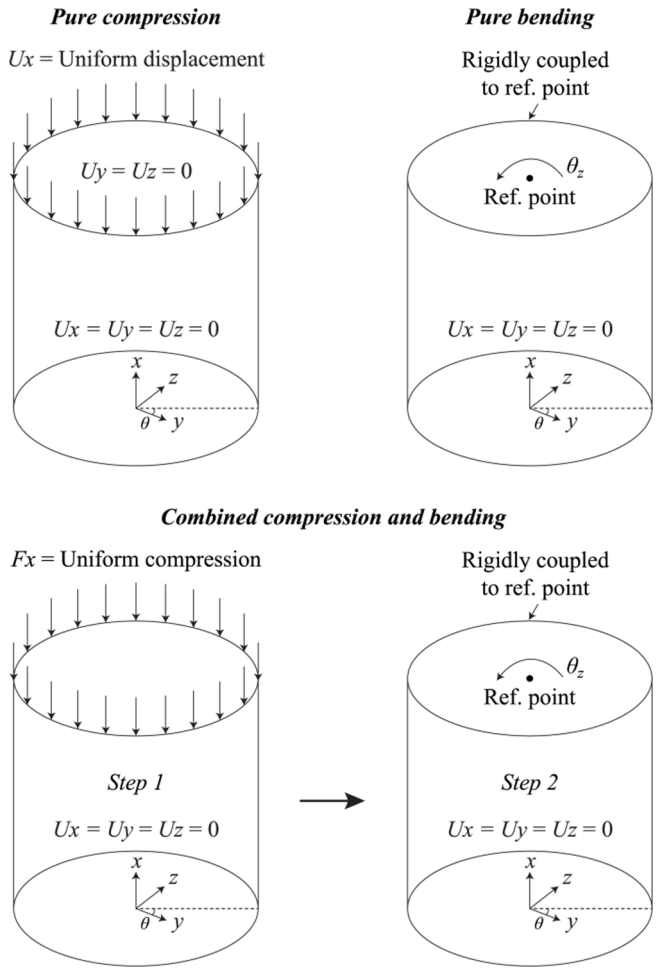

Fig. 6. Schematics of boundary condition and load application of finite element model.

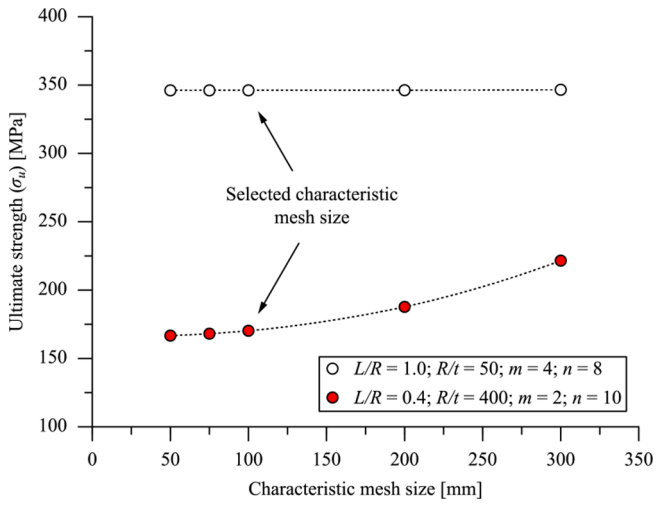

Fig. 7. Mesh convergence study.

imperfection magnitude; l is the length of the unstiffened shell or spacing between ring stiffeners; m is the number of half wave in the longitudinal direction; n is the number of full waves in the circumferential direction. In this paper, the imperfection shape (i.e., m & n) is determined based on a linear buckling analysis from which the first order eigenmode is utilised. The first order eigenmode was adopted because it is usually the governing buckling mode shape that leads to collapse of the cylindrical shell, although the actual as-built imperfection might be a weighted combination of different mode shapes and the first order eigenmode may not provide the worst-case scenario. In general, the first order eigenmodes are of two forms, i.e., non-rotational-symmetric and rotational-symmetric. In the former case, the cylindrical shell deflects in both longitudinal and circumferential directions (non-zero m & n). However, in the latter case, the cylindrical shell only deflects in the longitudinal direction and there is no variation in the circumferential direction (i.e., $n = 0$). As summarised in Table 2, non-rotational-symmetric eigenmode usually occurs in stocky cylindrical shells, and the rotational-symmetric eigenmode usually presents in slender cylindrical shells. An example illustration of these two eigenmodes is given in Fig. 5 with a magnification factor of 50. The imperfection magnitude is determined by Equation (13) which was suggested in [46]. This specification of maximum imperfection magnitude is knock-down factor equivalent imperfection magnitude, i.e., the numerical simulation can give a buckling load equivalent to applying a knockdown factor to the classical buckling load in which the knock down factor is specified according to the NASA SP-8007 Space Vehicle Design Criteria.

$$w_{max}/t = 0.025\left(-2.8+\sqrt{R/t}\right) \tag{13}$$

As the primary objective of this paper is to demonstrate and verify the proposed fibre-based modelling, the above specifications of geometric imperfection are only referencing values. Nevertheless, it was highlighted through experimental studies reported in [47–49] that the buckling strength of cylindrical shell is highly sensitive to geometric imperfection (both imperfection shape/distribution and magnitude). In the light of predicting lower bound buckling strength, worst multiple-perturbation load approach appears to be more suitable, as compared with the single perturbation approach. More rigorous evaluation of the effect of geometric imperfection may also refer to [50–53] and others. The effect of fabrication-induced residual stress is also ignored in this study. As explained, this is out of the scope of the present study. With regards to cylindrical shells, the fabrication-induced residual stress may be developed by cold bending and/or welding. The former is required to form a curve plate from flat sheet, while the latter is needed to assemble the cylindrical shell by longitudinally welding several curved plates. In the case of ring-stiffened cylindrical shells, additional welding is required for joining the ring stiffeners onto the shell structures. Dedicated research in this aspect may refer to [42,54].

In terms of the boundary condition and loading application for finite element modelling, a schematic illustration is provided in Fig. 6. For simulating the response under pure compression, both ends of the cylindrical shell was simply supported. Axial displacement was applied to one end of the model via a reference point coupled to all nodes at the model end. This allowed a uniform displacement application and kept the loaded edge straight. For predicting the response under pure bending, simple support was considered at the unloaded end, and the loaded end was rigidly coupled to the reference point in which the rotational displacement was applied. With the loaded edge modelled as rigid, unrealistic local deformation can be avoided. Moreover, this modelling technique allows the translational movement of the load application point so as to simulate the progressive movement of the instantaneous neutral axis. For combined compression and bending, a two-step approach was adopted. In the first step, the uniform compressive force was applied as pre-loading. Whilst the boundary condition at the unloaded end was consistent with that in the pure compression case, the loaded edge was set to be free. This is due to the fact that the simulation of the neutral axis movement cannot be simulated in the second step as a result of the fixed loaded edge. However, as the pre-loaded compression does not exceed the ultimate limit, the free boundary in the first step should not result in a substantial inconsistency between the combined load case and the pure load case.

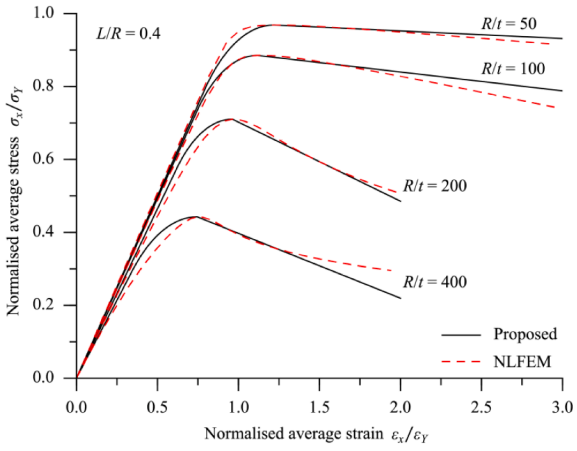

(a). $L/R = 0.4$

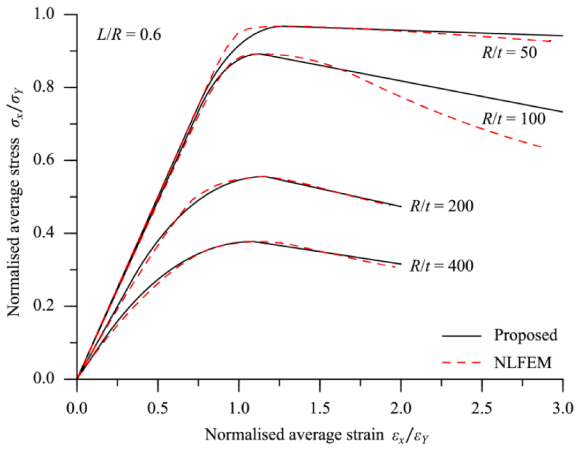

(b). $L/R = 0.6$

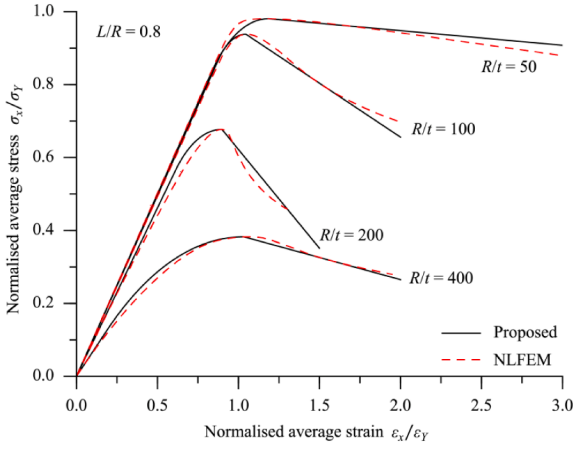

(c). $L/R = 0.8$

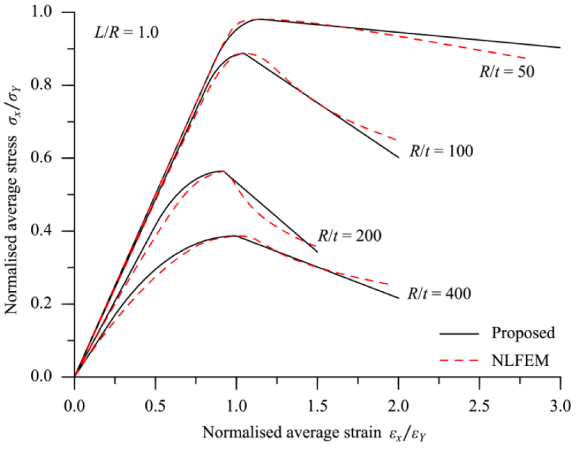

(d) $L/R = 1.0$

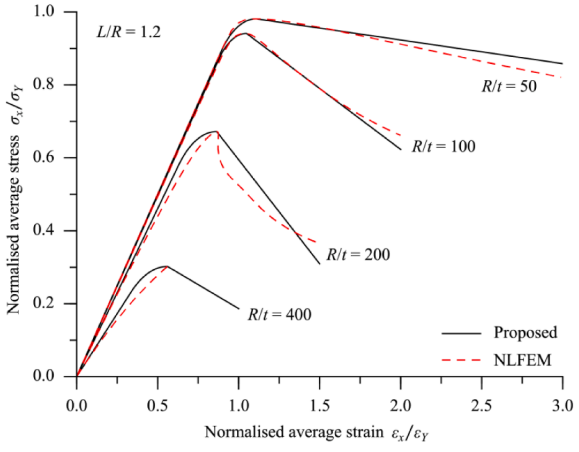

(e) L/R = 1.2

Fig. 8. Comparison of load-shortening curves under pure compression.

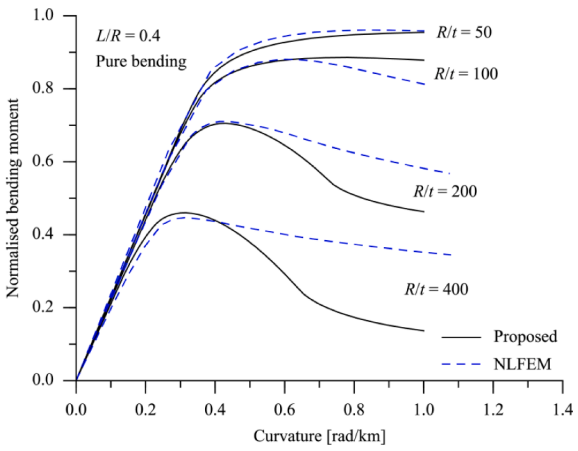

(a). $L/R = 0.4$

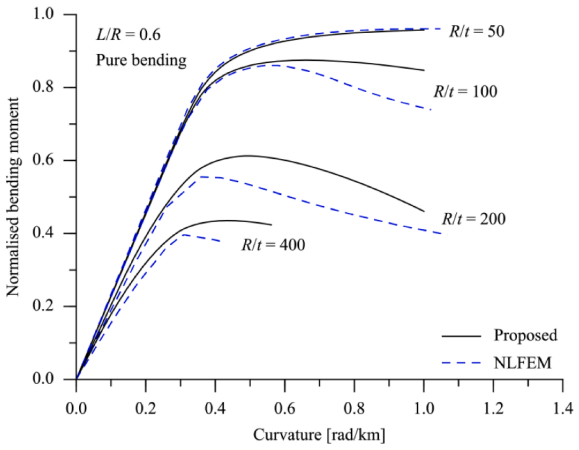

(b). $L/R = 0.6$

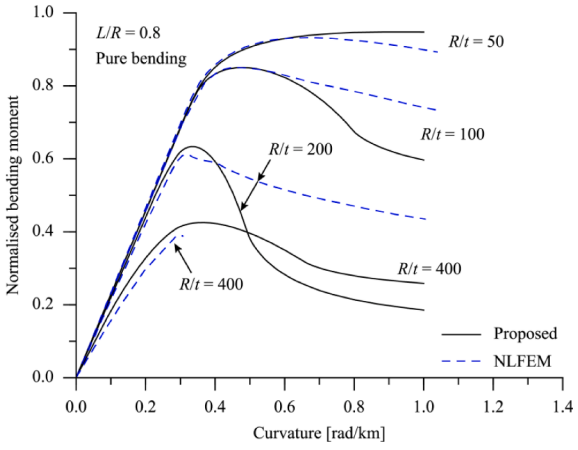

(c). $L/R = 0.8$

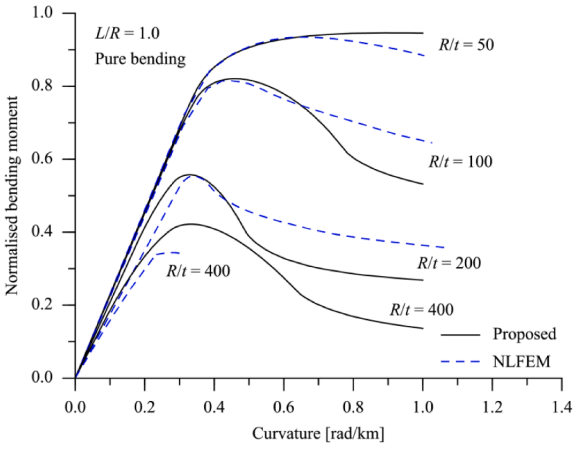

(d). $L/R = 1.0$

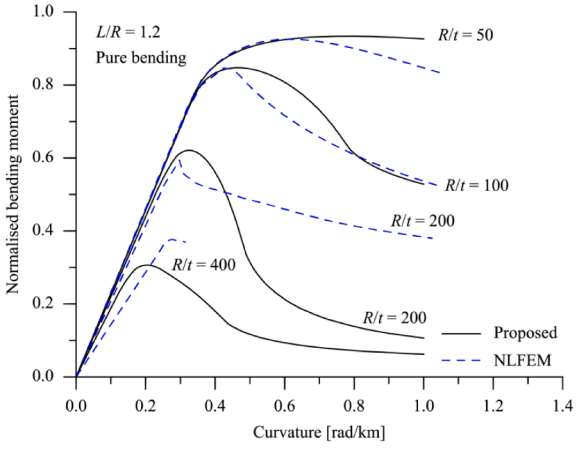

(e) $(L/R = 1.2)$

Fig. 9. Comparison of bending moment versus curvature curves (Pure bending).

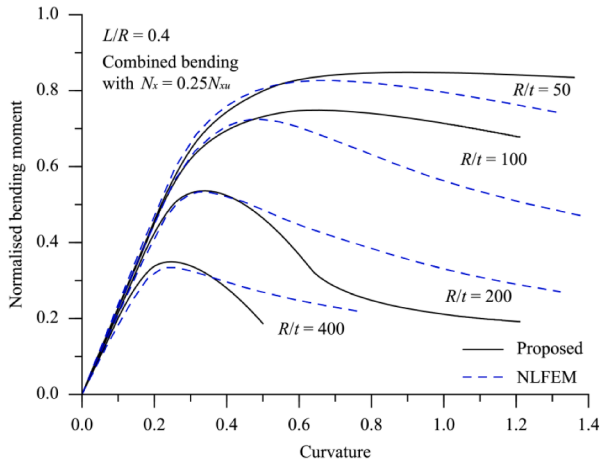

(a) ($L/R = 0.4$)

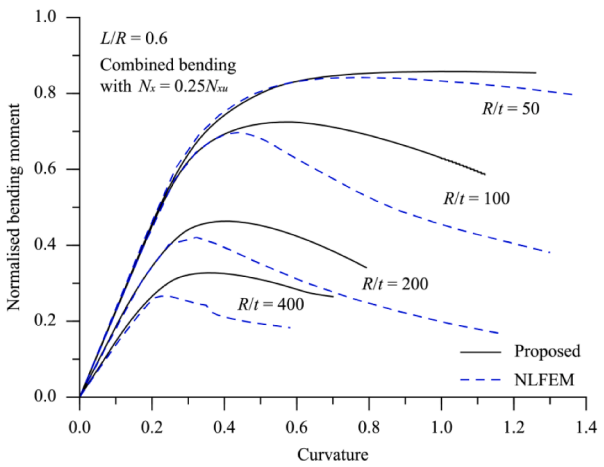

(b) ($L/R = 0.6$)

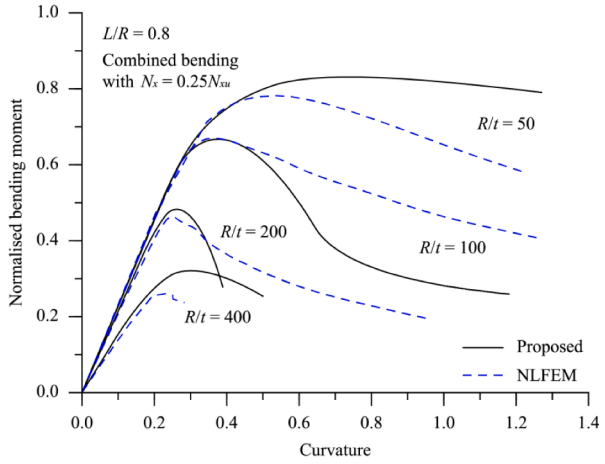

(c) ($L/R = 0.8$)

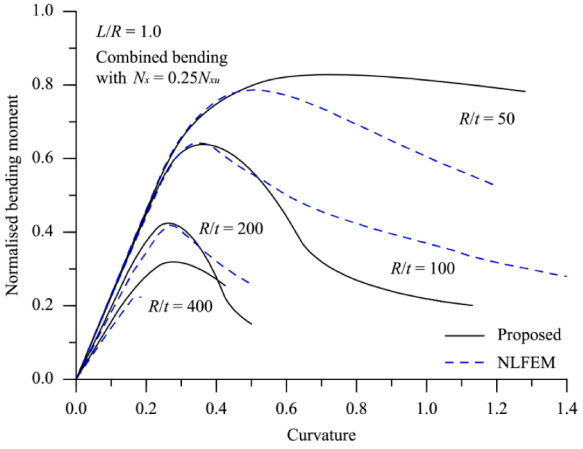

(d) ($L/R = 1.0$)

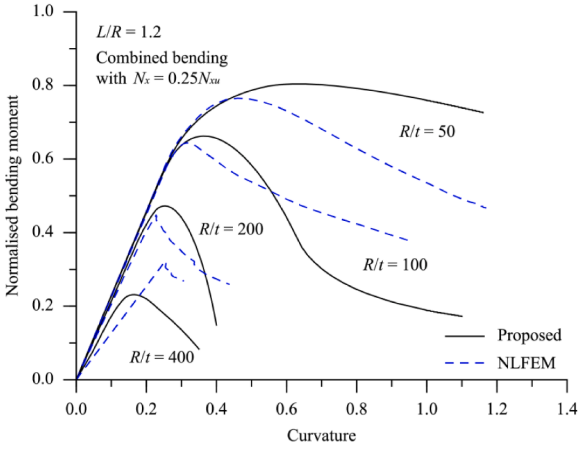

(e) ($L/R = 1.2$)

Fig. 10. Comparison of bending moment versus curvature curves (Combined bending and axial compression with $N_x/N_{xu} = 0.25$).

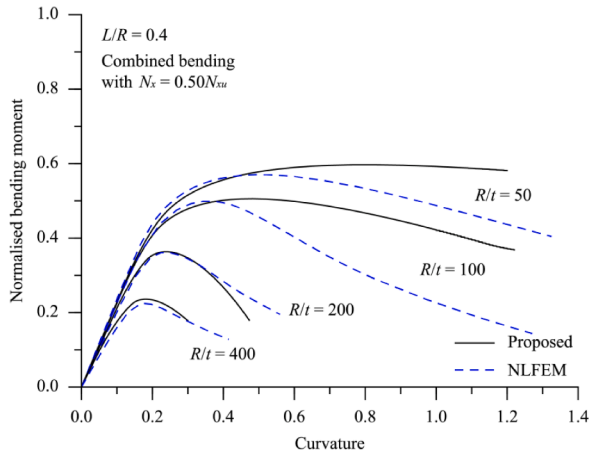

(a) ($L/R = 0.4$)

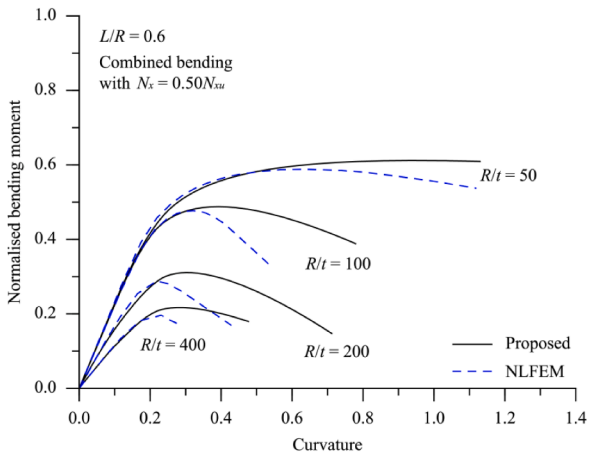

(b) ($L/R = 0.6$)

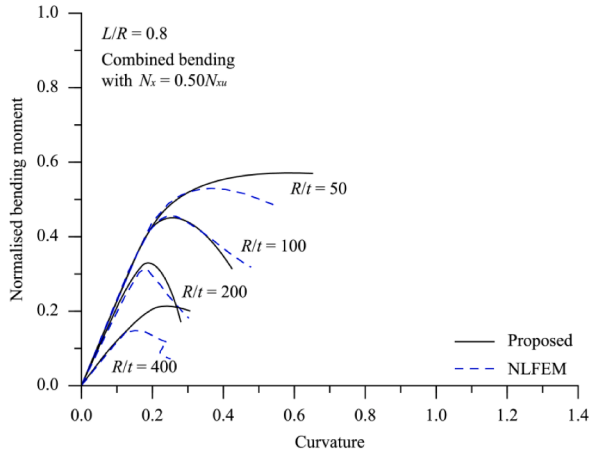

(c) ($L/R = 0.8$)

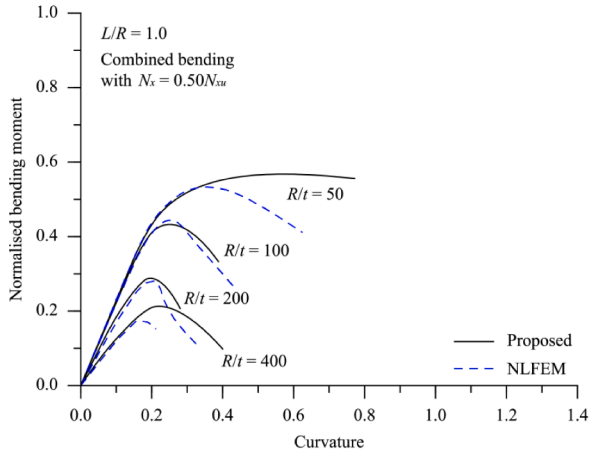

(d) ($L/R = 1.0$)

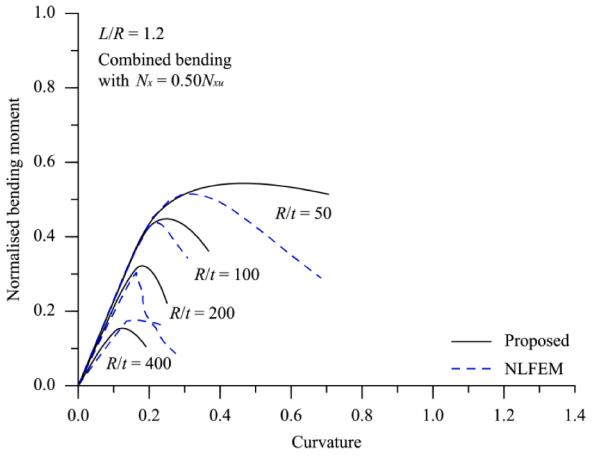

(e) ($L/R = 1.2$)

Fig. 11. Comparison of bending moment versus curvature curves (Combined bending and axial compression with $N_x/N_{xu} = 0.50$).

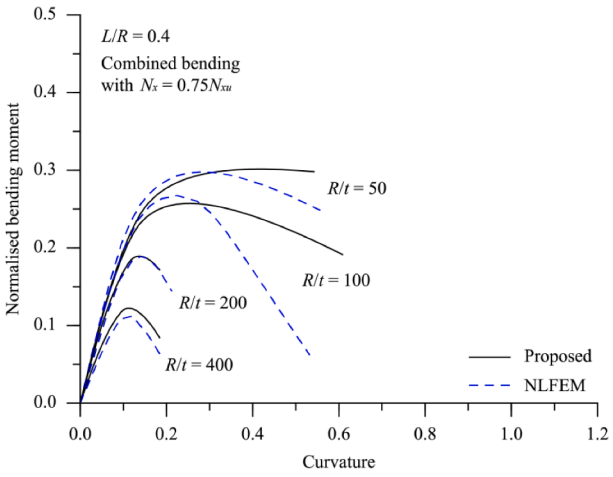

(a) ($L/R = 0.4$)

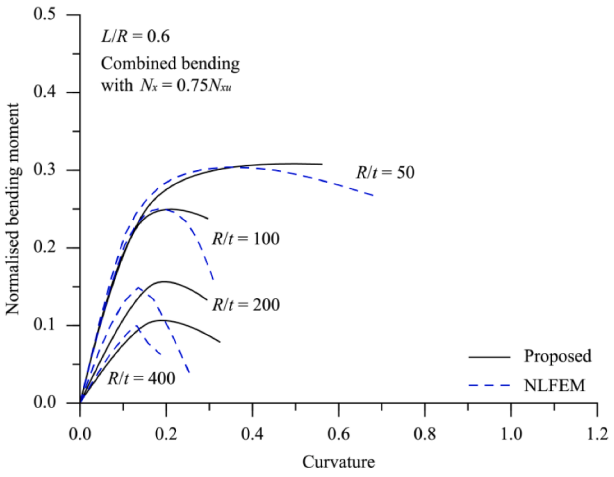

(b) ($L/R = 0.6$)

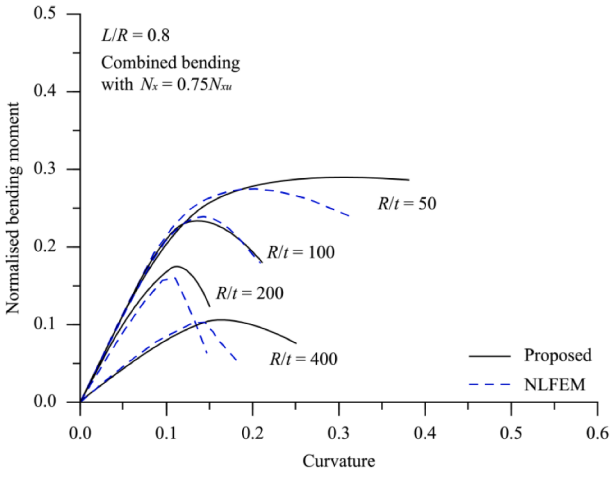

(c) ($L/R = 0.8$)

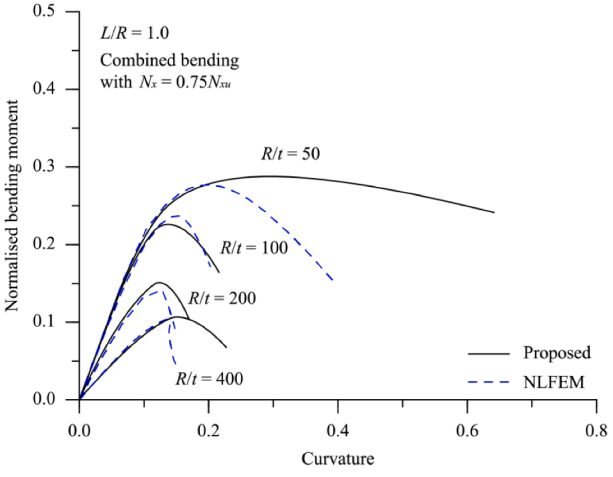

(d) ($L/R = 1.0$)

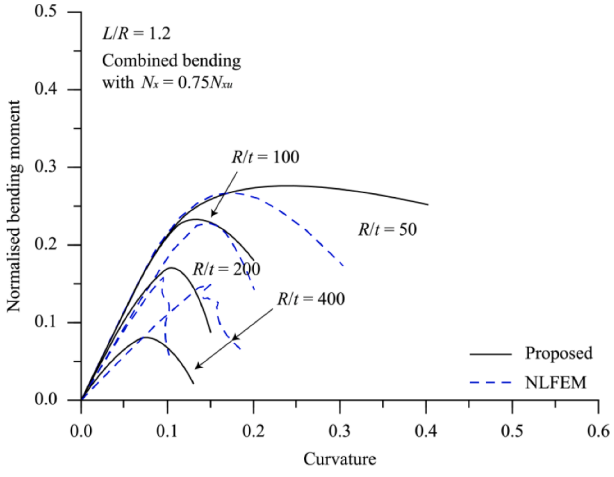

(e) ($L/R = 1.2$)

Fig. 12. Comparison of bending moment versus curvature curves (Combined bending and axial compression with $N_x/N_{xu} = 0.75$).

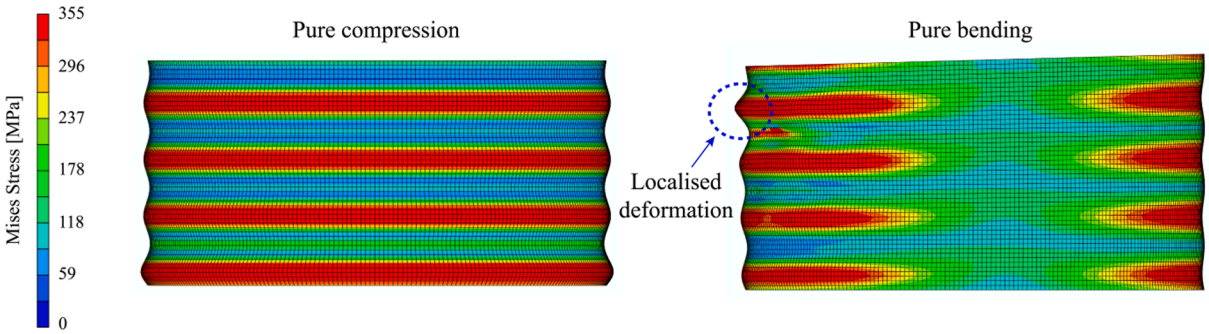

Fig. 13. Comparison of buckling modes in compression and bending moment of cylindrical shell with rotational-symmetric initial geometric imperfection.

The mesh density also has a great influence on the collapse analysis of thin-walled structures. To this end, a mesh convergence study has been completed for the pure axial compression case. Different mesh densities were considered, with characteristic element sizes ranging from 50 mm × 50 mm to 300 mm × 300 mm. As shown in Fig. 7, the change in characteristic mesh size does not result in a significant variation in the predicted ultimate compressive strength of the stocky cylindrical shell with $L/R = 1.0$ and $R/t = 50$. Conversely, a finer mesh leads to a smaller ultimate compressive strength prediction of a slender cylindrical shell with $L/R = 0.4$ and $R/t = 400$. The effect of mesh size converges when it is smaller than 100 mm × 100 mm. In the light of achieving reliable numerical prediction and reducing the computational cost, the mesh size 100 mm × 100 mm was adopted for the remaining analyses of this study.

4.3. Results

4.3.1. Comparison of Load-shortening curves under pure compression

The characteristic load-shortening features, i.e., initial stiffness, ultimate strength, ultimate strain, and post-collapse stiffness, have been predicted by nonlinear finite element method and fed into the proposed empirical load-shortening formulation. In future work, a more dedicated analytical or data-driven approach can be utilised for deriving these characteristic features. However, this is out of the scope of the present paper.

A comparison between the compressive load-shortening curves predicted by the nonlinear finite element method and the proposed empirical method is shown in Fig. 8. The pre-collapse regime of small radius-to-thickness ratio (i.e., stocky models) generally exhibits a linear response with an initial stiffness close to the material elastic modulus. This linear response would remain until a high load level, after which the load-shortening curve approaches the ultimate limit state with a relatively distinct transition. By contrast, the initial stiffness of large radius-to-thickness ratio cylindrical shells (i.e., slender models) shows a much lower value and gradually decreases until collapse as the axial compression is increased. The collapse of the cylindrical shells generally occurs with an ultimate strain close to the material yield strain. In terms of the post-collapse regime, the unloading response and post-collapse stiffness appears to be affected by the length-to-radius ratio. Regarding the cylindrical shell with small length-to-radius ratio, the post-collapse regime shows a less significant unloading. Conversely, there is great post-collapse unloading when it comes to cylindrical shells with large length-to-radius ratio. This is likely because of the localisation of buckling deformation in the post-collapse regime. In the pre-collapse regime, the buckling deformation develops generally following the initial geometric imperfection shape. After the ultimate collapse, the structural deformation will nucleate in localised region which reflects as steep post-collapse unloading in the load-shortening curve. The load–displacement response predicted by the proposed fibre formulation is closely correlated with that computed by the nonlinear finite element method. The largest discrepancy occurs in the post-collapse range. However, the prediction of post-collapse response has always been

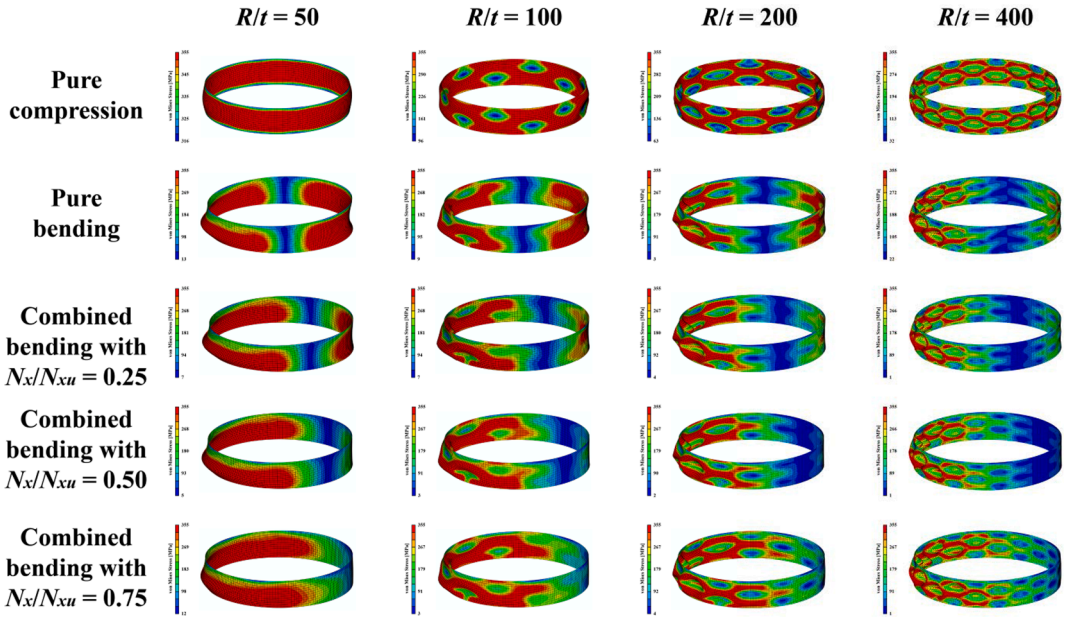

Fig. A1. Deformation contour plots of cylindrical shells at ultimate limit state ($L/R = 0.4$).

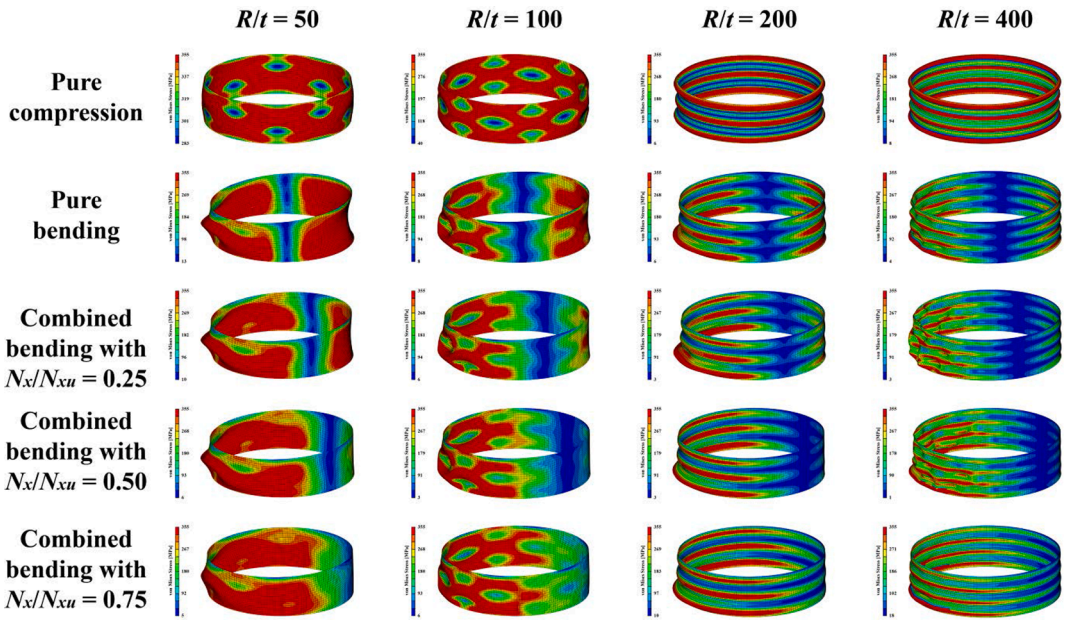

Fig. A2. Deformation contour plots of cylindrical shells at ultimate limit state ($L/R = 0.6$).

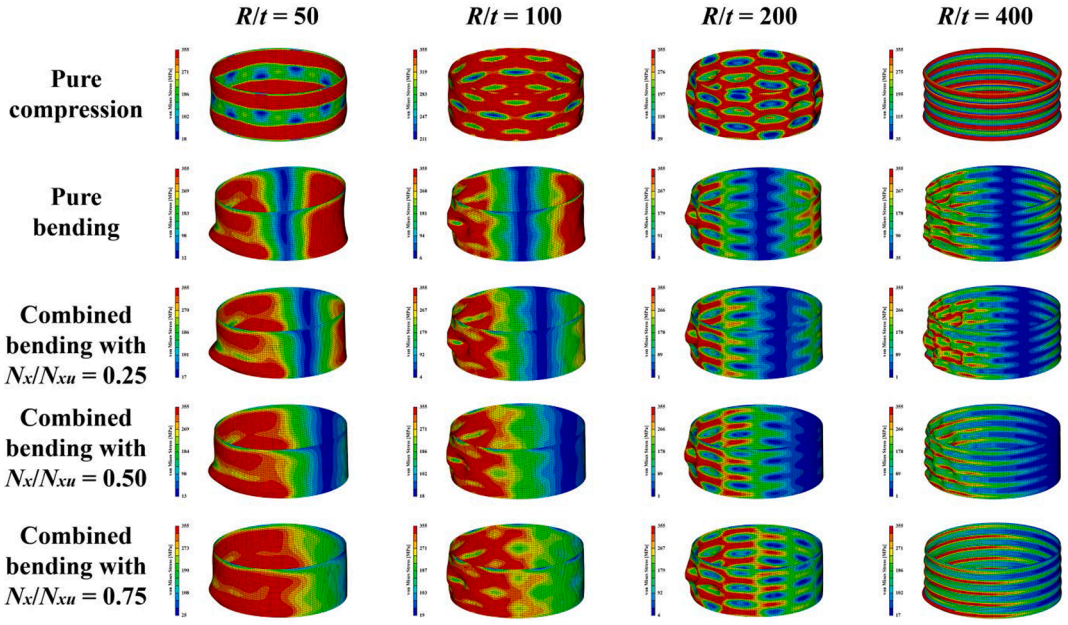

Fig. A3. Deformation contour plots of cylindrical shells at ultimate limit state ($L/R = 0.8$).

challenging, as it is governed by many interacting parameters such as slenderness, imperfection shape, imperfection magnitude and numerical solvers in the context of finite element analysis. For instance, it was reported by [53] and [55] that the use of the preferred buckling mode as the imperfection shape could lead to a non-conservative prediction of the post-collapse unloading. Further analysis will be presented in the following section to examine the effect of load-shortening curve formulation. A comprehensive examination of the effect of load-shortening curves on the ultimate bending strength of stiffened plated hull girders was given in [56].

4.3.2. *Comparison of bending moment versus curvature curves*

The comparison of bending moment versus curvature relation predicted by the proposed fibre-based modelling and nonlinear finite element method is shown in Figs. 9, 10, 11 and 12 for the pure bending load case, combined load case with pre-compression of $N_x/N_{xu} = 0.25$, $N_x/N_{xu} = 0.50$ and $N_x/N_{xu} = 0.75$ respectively. Note that the bending moment shown in Figs. 9 to 12 is normalised by the corresponding plastic bending moment, excluding the effect of buckling. The pre-collapse responses in most cases are reasonably correlated between the two methods, except for the long and slender cylindrical shells under a pure bending moment (e.g., $L/R = 1.0$ & $R/t = 200$; $L/R = 1.0$ & $R/t = 400$; $L/R = 1.2$ & $R/t = 400$). In these cases, the fibre element-based method noticeably overestimates the pre-collapse response as compared with that predicted by finite element method. This is likely due to the change in the buckling mode of these shell structures (Fig. 13). Under pure compression, these structures show a rotational-symmetric deflection mode which would give a higher axial stiffness to the shell model. Thus, the underpinning load-shortening response used in the fibre-based method is embedded with higher axial stiffness.

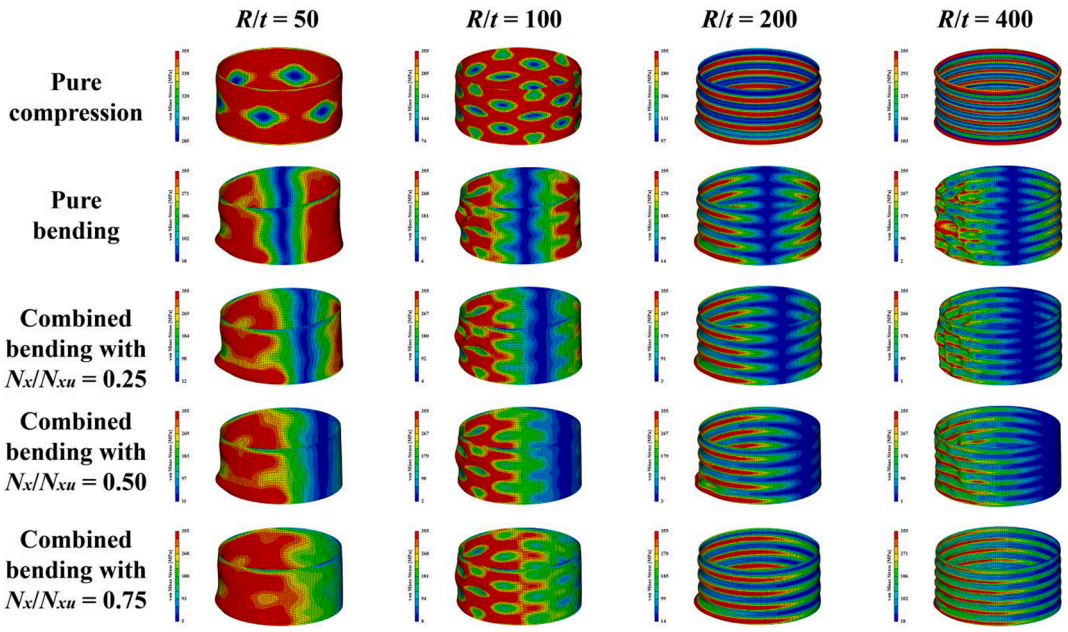

Fig. A4. Deformation contour plots of cylindrical shells at ultimate limit state ($L/R = 1.0$).

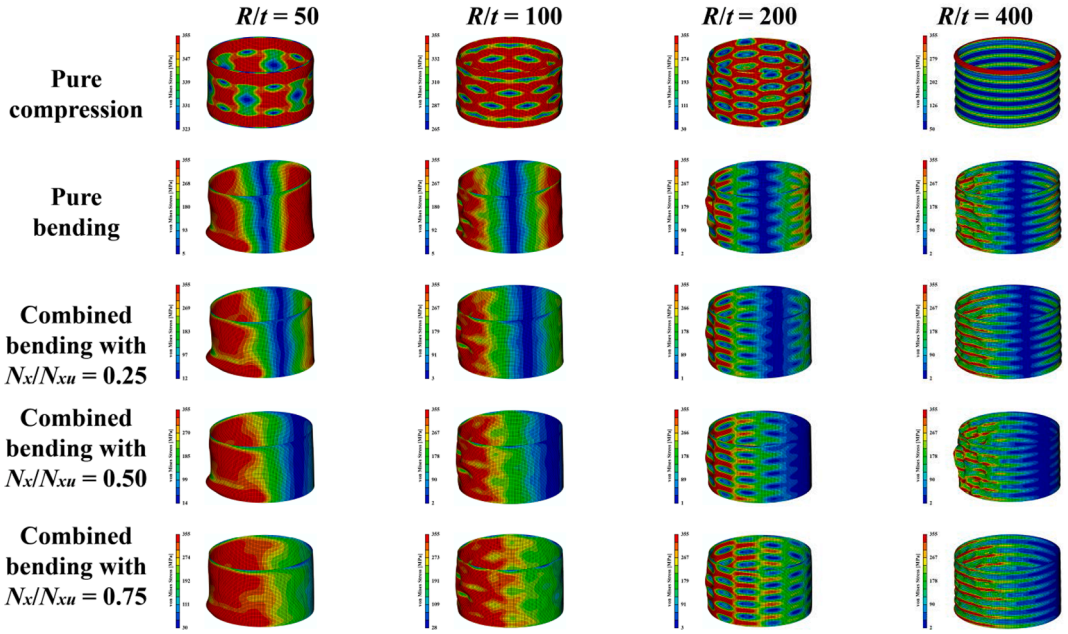

Fig. A5. Deformation contour plots of cylindrical shells at ultimate limit state ($L/R = 1.2$).

By contrast, localised deformation is found when the shell structure is subjected to bending load, which eventually leads to a different collapse mode and would generally give a less stiff response. This discrepancy suggests that the derivation of the axial load-shortening curve of fibre element should consider the difference in buckling failure mode between compression and bending. In the meantime, it may be deduced that the sensitivity of cylindrical shells to geometric imperfection could differ between different load cases, even though the governing failure mode is compressive buckling. Comparison of the deformation contour plots of all cylindrical shell models are shown in the Appendix for different load cases (Figs. A1, A2, A3, A4, A5).

The difference in the post-collapse response is relatively obvious. This discrepancy can be caused by a number of factors, such as the boundary condition and the numerical solver. When it comes to the pure bending load case, the difference is likely affected by the boundary condition specified in the present finite element model. As a single bay model is adopted, the boundary constraint may have a great influence on the deformation localisation in the post-collapse range. Thus, if the present finite element model was to be the representation of a ring-stiffened cylindrical shell (assuming no failure in the ring stiffeners), the present finite element prediction of the post-collapse unloading might be optimistic.

The correlation between the ultimate bending strength predicted by the nonlinear finite element method and fibre-based modelling for cylindrical shells is shown in Fig. 14, in which the sensitivities to load case, radius-to-thickness ratio and length-to-radius ratio are highlighted. The overall bias and coefficient of variation (COV) between the two approaches are 0.98 and 0.13, respectively, which indicates high accuracy

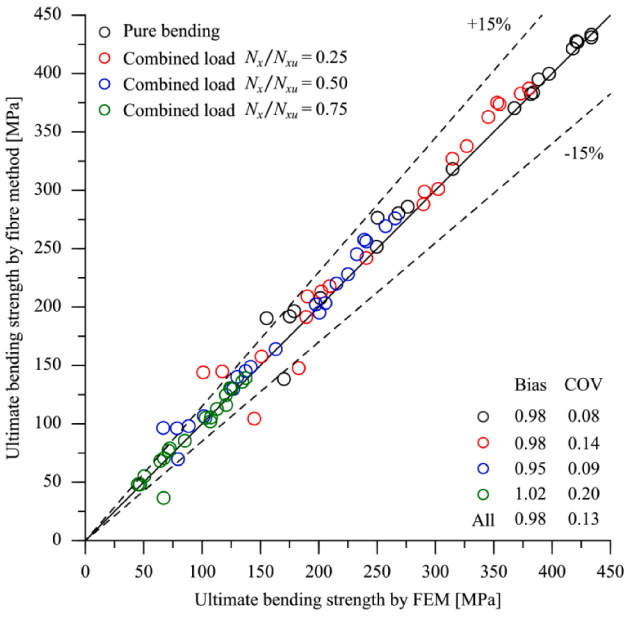

(a). Different load cases

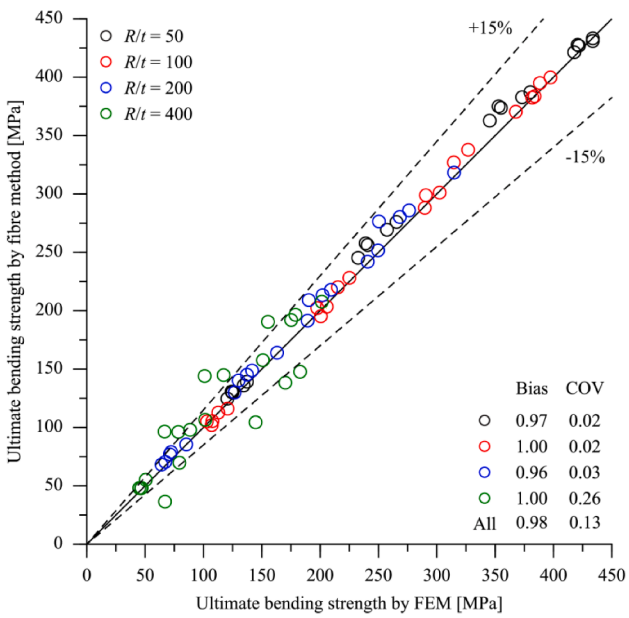

(b). Different radius-to-thickness ratio

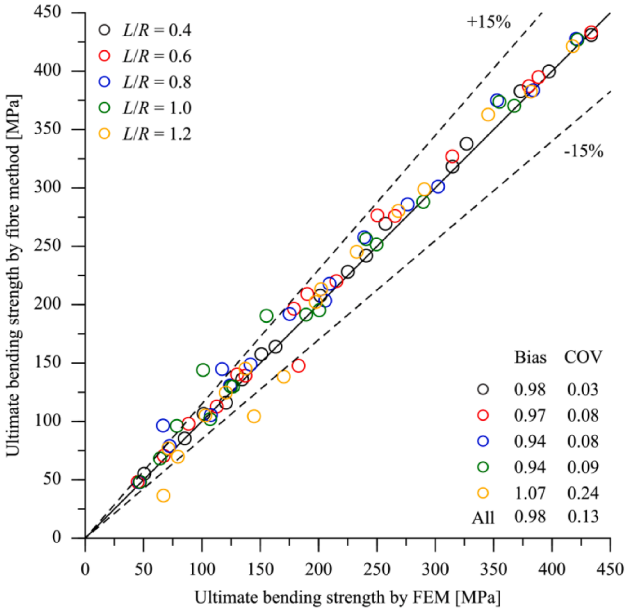

(c) Different length-to-radius ratios

Fig. 14. Correlation between the ultimate bending strength predicted by finite element method (FEM) and fibre-based modelling for cylindrical shells.

of the proposed fibre-based modelling with reference to the nonlinear finite element method. The prediction bias in all cases, i.e., different load cases, radius-to-thickness ratios and length-to-radius ratios, is in the range of 0.95 to 1.07. However, a larger prediction scattering is observed in the case of high pre-loaded compression (COV = 0.20), large radius-to-thickness ratio (COV = 0.26) or large length-to-radius ratio (COV = 0.24). In all these scenarios, it appears that convergence is difficult to achieve in the finite element simulations, as the cylindrical shells experience a fairly unstable load–displacement path. Further validation is required, in particular a dedicated experimental programme, to demonstrate and verify the capability of the fibre-based modelling for these highly nonlinear cases. Nevertheless, it can be concluded that the proposed fibre-based method is well suited for predicting the ultimate strength of stocky cylindrical shells predominately under bending moment with moderate pre-loaded compression. This appears to be a common scenario in the maritime sector, such as the offshore wind structures where the turbine and nacelle induce pre-loaded compression to offshore support foundation, and the combination of wind/wave/current force induces a bending moment.

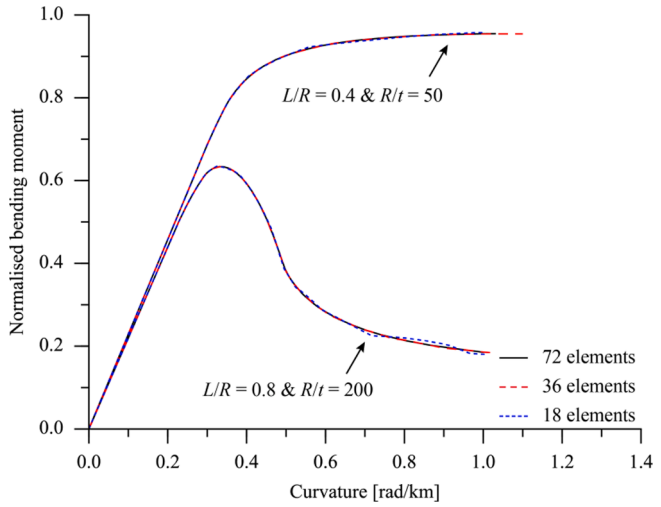

Fig. 15. Comparison of bending moment versus curvature curves based on different numbers of fibre elements.

5. Parametric study

5.1. Effect of fibre element size

In the previous section, 72 fibre elements were used to mesh the cross section of the cylindrical shell. In this section, the effect of fibre element size is examined. A selection of the bending moment versus curvature curves predicted by different numbers of fibre elements (18, 36 and 72 elements) are shown in Fig. 15. Note that the illustrated comparison is typical across all cases. The effect of fibre element size appears to be negligible. There is virtually no difference in the simulation of the initial response and ultimate strength. As a recommended practice, a smaller number of fibre element may be more efficient whilst the accuracy is not degraded. This reduction in computational time can be significant for a large amount of calculation iteration, such as reliability assessment and structural optimisation. Nevertheless, if one is interested in the progressive collapse behaviour of each element with a higher resolution, a smaller fibre element size should be adopted.

5.2. Effect of local response modelling

As shown in Figs. 9 to 12, the prediction of post-collapse behaviour is the largest discrepancy in the load-shortening curves predicted by the finite element method and the empirical local response formulation. In light of this, the local response modelling, in particular the post-collapse response, is examined in this section. Fig. 16 shows the comparison of bending moment versus curvature curves predicted by the fibre-based model using different load-shortening curve inputs for two cylindrical shells. It is clear that the progressive bending collapse response of stocky shell (e.g., $L/R = 1.0$ & $R/t = 50$) is relatively insensitive to the load-shortening curve input. However, the plastic bending moment, in this case, is still an appreciable overestimation compared with the ultimate bending moment considering buckling/plastic effect. The progressive collapse behaviour of slender shell (e.g., $L/R = 0.6$ & $R/t = 400$) is highly sensitive to the load-shortening curve input. The plastic bending moment is unrealistically optimistic in this scenario. If the load-shortening curve is incorporated with a perfectly plastic post-collapse response (i.e., without post-collapse unloading), the global structural system would not experience a clear ultimate limit state, despite the fact that the pre-collapse response is identical. This comparison suggests that the progressive collapse behaviour and ultimate strength prediction of slender cylindrical shells might be associated with a high degree of uncertainty, if different formulations load-shortening curves are employed. This observation aligns with that found in the stiffened plated

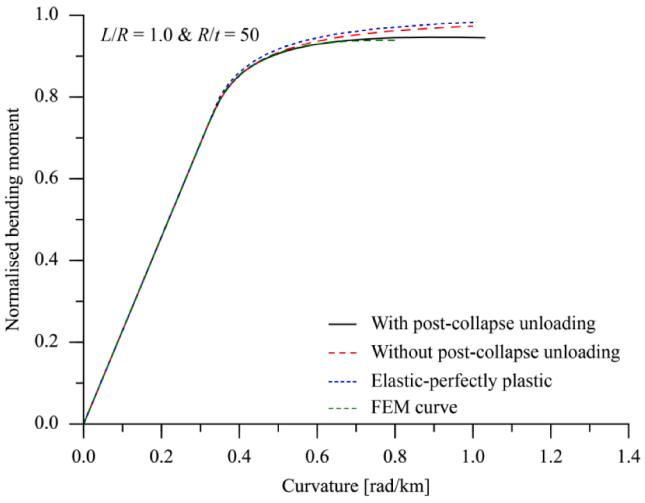

(a). $L/R = 1.0$ & $R/t = 50$

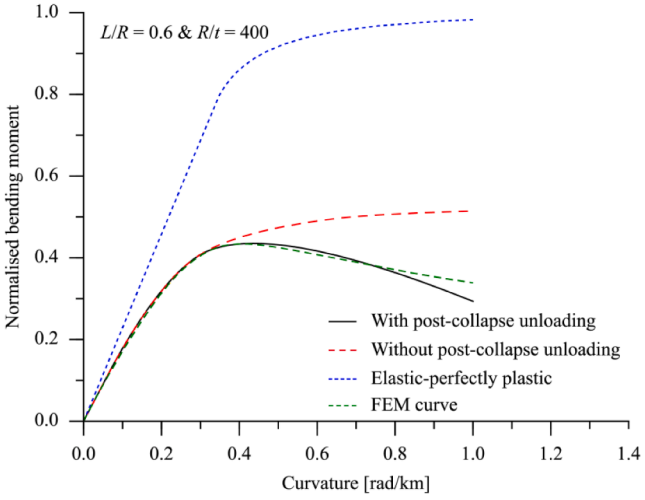

(b). $L/R = 0.6$ & $R/t = 400$

Fig. 16. Comparison of bending moment versus curvature curves predicted by different load-shortening curve formulations.

structures [53]. In addition, it should be remarked that the bending moment versus curvature curves predicted by the proposed load-shortening curve formulation and FEM are well compared. This may further demonstrate the rationality of the proposed formulation.

5.3. Comparison with codified methods

A comparison between the fibre-based model, NLFEM and code formulae for predicting the ultimate bending strength are shown in Fig. 17 for the ultimate bending strength of cylindrical shells. The prediction is compared only for the cylindrical shell of $L/R = 0.4$, since the code formulae is insensitive to the length-to-radius ratio. In the meantime, the ultimate bending strength is expressed in terms of a quasi-elastic manner based on elementary beam theory, as follows:

$$\sigma_{xu,b} = M_u/\pi R^2 t \tag{14}$$

This is because all the code formulae are given in terms of bending stress. It can be seen from the comparison that the code formulae may be

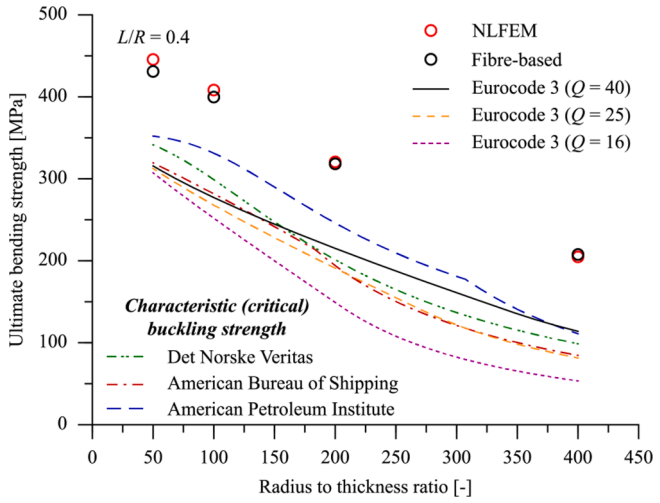

Fig. 17. Comparison of ultimate bending strength between proposed method, NLFEM and code formulae.

overly conservative with respect to NLFEM and the proposed method. Whist the difference in the embedded imperfection in different approaches causes uncertainty. The prediction discrepancy is likely due to the neglection of load-shedding during the progressive collapse of the cylindrical shell under global bending since most formulae assume that the entire collapse would occur when the outer fibre of the cylindrical shell fails. However, the shell structures still have the reserved effectiveness to bear additional loads due to the load-shedding from collapsed element to intact element.

6. Conclusions

This paper has presented a fibre-based model for predicting the ultimate strength of cylindrical shells under combined axial compression and bending moment. The fibre-based model evaluates the progressive collapse behaviour by accounting for the contribution of local fibre element to the global structural system. The local response of the fibre element is encapsulated in a load-shortening curve which characterises its behaviour under longitudinal load effects. In this paper, an efficient empirical formulation has been applied to estimate the load-shortening curve of fibre elements. Validation has been completed using the equivalent nonlinear finite element method on a parametric range of cylindrical shell models and load combinations. The following conclusions are drawn from this paper:

- With reference to the equivalent nonlinear finite element method, the proposed fibre-based model shows an overall bias of 0.98 and COV of 0.13. This indicates its reasonably high accuracy and acceptable prediction scattering. Thus, the proposed fibre-based model can be concluded as a capable method to evaluate the progressive collapse and ultimate strength of cylindrical shell structures under combined axial compression and bending.
- The largest prediction discrepancy is found in the cases with high pre-loaded compression, large radius-to-thickness ratio, or large length-to-radius ratio. In fact, the finite element simulation for these scenarios is susceptible to the convergence issue. Hence, to validate the capability of the proposed method, more dedicated investigation in particular experimental studies is required in the future.
- The local response formulation provides an efficient and robust way to estimate the load-shortening curve of cylindrical shells with acceptable accuracy, provided that the four response characteristics, i.e., initial stiffness, ultimate strength, ultimate strain and post-collapse stiffness, can be reasonably estimated.
- The effect of fibre element size appears to be a non-critical issue. Thus, as a recommended practice, a smaller element size may be adopted. This could potentially benefit structural reliability analysis and structural optimisation, in which case a large number of iterations is needed.
- The code formulae prediction seems to be overly conservative with respect to NLFEM and the proposed method. The difference in the embedded imperfection in different approaches causes uncertainty. The prediction discrepancy is likely due to the neglection of load-shedding during the progressive collapse of cylindrical shell under global bending, since most formulae assume that the entire collapse would occur when the outer fibre of the cylindrical shell fails.

The present study has in principle proven the validity of fibre-based method to model the progressive collapse and ultimate strength of cylindrical shells under combined compression and bending moment. To further refine this methodology and extend its capability, the following further works may be considered:

- The sensitivity to geometric imperfection should be further evaluated, especially for cylindrical shells with different critical buckling modes under axial compression and bending moment, i.e., slender structures. As shown by the present numerical results, the same cylindrical shell structure will show a different buckling mode when subjected to bending moment, even though the initial geometric imperfection shape is specified in accordance with the first order eigenmode under pure axial compression. This implies that the derivation of elemental load-shortening curves should take into account of the difference due to the change of buckling mode shape.
- The local response formulation should be refined with the aid of a data-driven approach to estimate the response characteristics. In this regard, many data analysis techniques can be employed, from simple regression to dedicated machine learning algorithms. With this data-driven model, the local response formulation can eliminate the use of numerical simulation, which further improves the computational efficiency.
- The present fibre-based model is validated for bending and combined compression and bending. In the maritime sector, the effect of hydrostatic pressure should be considered. Future studies can be directed to incorporate hydrostatic pressure into the proposed computational scheme.
- The proposed model is currently limited to the prediction of cross-sectional behaviour. Whilst this is sufficient for ordinary design assessment (e.g., assessing the ultimate strength), one may be interested in the global deformation of the entire cylinder. In this regard, a hybrid formulation incorporating the fibre-based method with a finite beam element framework would be a promising solution. The concept was applied by Li et al. [57] for stiffened plated girder, and similar development can be completed for cylindrical shell structures in the future.

CRediT authorship contribution statement

Shen Li: Conceptualization, Methodology, Software, Validation, Formal analysis, Investigation, Writing – original draft, Writing – review & editing, Visualization. **Do Kyun Kim:** Conceptualization, Methodology, Writing – original draft, Writing – review & editing, Visualization, Supervision, Funding acquisition. **Qing Quan Liang:** Conceptualization, Methodology, Writing – original draft, Writing – review & editing, Visualization, Supervision.

Declaration of Competing Interest

The authors declare that they have no known competing financial interests or personal relationships that could have appeared to influence

the work reported in this paper.

Acknowledgement

This work was supported by the Basic Science Research program funded by the Ministry of Science and ICT through the National Research Foundation of Korea (NRF-2022R1F1A1065425).

References

[1] Paik JK. Advanced structural safety studies: with extreme conditions and accidents. Springer; 2020.
[2] DNVGL. Buckling strength of shells. DNVGL-RP-C202 2018.
[3] ABS, 2016. Guide for buckling and ultimate strength assessment for offshore structures (LRFD version).
[4] API, 2004. Bulletin on stability design of cylindrical shells.
[5] Eurocode 3, 2006. Design of steel structures – Part 1-6: Strength and stability of shell structures.
[6] Elchalakani M. A closed-form solution for elastic buckling of thin-walled unstiffened circular cylinders in pure flexure. Thin-Walled Struct 2014;80:120–9.
[7] Kim SE, Kim CS. Buckling strength of the cylindrical shell and tank subjected to axially compressive loads. Thin-Walled Struct 2002;40(4):329–53.
[8] Cerik BC. Ultimate strength of locally damaged steel stiffened cylinders under axial compression. Thin-Walled Struct 2015;95:138–51.
[9] Li S, Kim DK. Ultimate strength characteristics of unstiffened cylindrical shell in axial compression. Ocean Eng 2022;243:110253.
[10] Liang QQ. Performance-based analysis of concrete-filled steel tubular beam–columns, Part I: Theory and algorithms. J Constr Steel Res 2009;65(2):363–72.
[11] Liang QQ. Performance-based analysis of concrete-filled steel tubular beam–columns, Part II: Verification and applications. J Constr Steel Res 2009;65(2):351–62.
[12] Liang QQ. Nonlinear analysis of circular double-skin concrete-filled steel tubular columns under axial compression. Eng Struct 2017;131:639–50.
[13] Liang QQ. Numerical simulation of high strength circular double-skin concrete-filled steel tubular slender columns. Eng Struct 2018;168:205–17.
[14] Ahmed M, Liang QQ, Patel VI, Hadi MNS. Nonlinear analysis of square concrete-filled double steel tubular slender columns incorporating preload effects. Eng Struct 2020;207:110272.
[15] Rizwan M, Liang QQ, Hadi MNS. Fiber-based computational modeling of rectangular double-skin concrete-filled steel tubular short columns including local buckling. Eng Struct 2021;248:113268.
[16] Rizwan M, Liang QQ, Hadi MNS. Numerical analysis of rectangular double-skin concrete-filled steel tubular slender columns incorporating interaction buckling. Eng Struct 2021;245:112960.
[17] Phan DHH, Patel VI, Liang QQ, Abadi HA, Thai HT. Simulation of uniaxially compressed square ultra-high-strength concrete-filled steel tubular slender beam-columns. Eng Struct 2021;232:111795.
[18] Phan DHH, Patel VI, Liang QQ, Abadi HA, Thai HT. Numerical investigations of circular double-skin steel tubular slender beam-columns filled with ultra-high-strength concrete. Eng Struct 2022;254:113814.
[19] Ahmed M, Liang QQ, Hamoda A. Fiber element modeling of circular double-skin concrete-filled stainless-carbon steel tubular columns under axial load and bending. Adv Struct Eng 2022.
[20] Al-Jelawy HM, Mackie KR. Three-dimensional fiber-based models of precast and cast-in-place reinforced concrete columns. J Struct Eng 2022;148(3).
[21] Aldabagh S, Hossain F, Alam MS. Simplified predictive expressions of drift limit states for reinforced concrete circular bridge columns. J Struct Eng 2022;148(3).
[22] Dow, R.S., Smith, C.S., 1986. FABSTRAN: A computer program for frame and beam static and transient response analysis (Nonlinear). ARE report TR86205.
[23] IACS, 2019. Common structural rules for bulk carriers and oil tankers. International Association of Classification Societies.
[24] Smith, C.S., 1977. Influence of local compressive failure on ultimate longitudinal strength of a ship's hull. In Proceeding: International Symposium on Practical Design of Ships and other Floating Structures (PRADS 1977), Tokyo, Japan.
[25] Dow RS, Hugill RC, Clark JD, Smith CS. Evaluation of ultimate ship hull strength. In Proceeding: Extreme Load Response Symposium, Arlington, VA; 1981.
[26] Benson S, Downes J, Dow RS. Compartment level progressive collapse analysis of lightweight ship structures. Mar struct 2013;31:44–62.
[27] Benson S, Downes J, Dow RS. Overall buckling of lightweight stiffened panels using an adapted orthotropic plate method. Eng Struct 2015;85:107–17.
[28] Syrigou, M., Benson, S., Dow, R.S., 2018. Progressive collapse assessment of intact box girders under combined bending and torsional loads. In Proceeding: International Conference on Ships and Offshore Structures (ICSOS 2018), Gothenburg, Sweden.
[29] Li S, Hu Z, Benson S. Progressive collapse analysis of ship hull girders subjected to extreme cyclic bending. Mar struct 2020;73:102803.
[30] Li S, Hu Z, Benson S. An analytical method to predict the buckling and collapse behaviour of plates and stiffened panels under cyclic loading. Eng Struct 2019;199:109627.
[31] Tatsumi A, Htoo Ko HH, Fujikubo M. Ultimate strength of container ships subjected to combined hogging moment and bottom local loads, Part 2: An extension of Smith's method. Mar struct 2020;71:102738.
[32] Li S, Kim DK. A comparison of numerical methods for damage index based residual ultimate limit state assessment of grounded ship hulls. Thin-Walled Struct 2022;172:108854.
[33] Tekgoz M, Garbatov Y, Guedes Soares C. Strength assessment of an intact and damaged container ship subjected to asymmetrical bending loadings. Mar struct 2018;58:172–98.
[34] Li S, Kim DK, Benson S. A probabilistic approach to assess the computational uncertainty of ultimate strength of hull girders. Reliab Eng Syst Saf 2021;213:107688.
[35] Liu Y, Frangopol DM. Time-dependent reliability assessment of ship structures under progressive and shock deteriorations. Reliab Eng Syst Saf 2018;173:116–28.
[36] Paik JK. Ultimate limit state design of steel-plated structures. John Wiley Sons Inc.; 2018.
[37] Ueda Y, Rashed SMH. An ultimate transverse strength analysis of ship structures. J Soc Naval Architects of Japan 1974;136:309–24.
[38] Kim DK, Park DH, Kim HB, Kim BJ, Seo JK, Paik JK. Lateral pressure effects on the progressive hull collapse behaviour of a Suezmax-class tanker under vertical bending moments. Ocean Eng 2013;63:112–21.
[39] Kim DK, Pedersen PT, Paik JK, Kim HB, Zhang XM, Kim MS. Safety guidelines of ultimate hull girder strength for grounded container ships. Saf Sci 2014;59:46–54.
[40] Lee DH, Kim SJ, Lee MS, Paik JK. Ultimate limit state based design versus allowable working stress based design for box girder crane structures. Thin-Walled Struct 2019;134:491–507.
[41] Li S, Kim DK, Benson S. An adaptable algorithm to predict the load-shortening curves of stiffened panels in compression. Ships and Offshore Struct 2021;16(sup1):122–39.
[42] Cerik BC, Cho SR. Numerical investigation on the ultimate strength of stiffened cylindrical shells considering residual stresses and shakedown. J Mar Sci Technol 2013;18:524–34.
[43] Shiomitsu D, Yanagihara D. Elastic local shell and stiffener-tripping buckling strength of ring-stiffened cylindrical shells under external pressure. Thin-Walled Struct 2020;148:106622.
[44] Shiomitsu D, Yanagihara D. Estimation of ultimate strength of ring-stiffened cylindrical shells under external pressure with local shell buckling or torsional buckling of stiffeners. Thin-Walled Struct 2021;161:107416.
[45] Yeter B, Garbatov Y, Guedes Soares C. Numerical and experimental study of the ultimate strength of a monopile structure. Eng Struct 2019;194:290–9.
[46] Friedrich L, Schmid-Fuertes TA, UweSchröder K. Comparison of theoretical approaches to account for geometrical imperfections of unstiffened isotropic thin walled cylindrical shell structures under axial compression. Thin-Walled Struct 2015;92:1–9.
[47] Wang B, Zhu SY, Hao P, Bi XJ, Du KF, Chen BG, et al. Buckling of quasi-perfect cylindrical shell under axial compression: a combined experimental and numerical investigation. Int J Solids Struct 2018;130–131:232–47.
[48] Wang B, Du KF, Hao P, Tian K, Chao YJ, Jiang LL, et al. Experimental validation of cylindrical shells under axial compression for improved knockdown factors. Int J Solids Struct 2019;164:37–51.
[49] Wang B, Ma XT, Hao P, Sun Y, Tian K, Li G, et al. Improved knockdown factors for composite cylindrical shells with delamination and geometric imperfections. Compos B Eng 2019;163:314–23.
[50] Hao P, Wang B, Li G, Meng Z, Tian K, Zeng DJ, et al. Worst Multiple Perturbation Load Approach of stiffened shells with and without cutouts for improved knockdown factors. Thin-Walled Struct 2014;82:321–30.
[51] Hao P, Wang B, Tian K, Du KF, Zhang X. Influence of imperfection distributions for cylindrical stiffened shells with weld lands. Thin-Walled Struct 2015;93:177–87.
[52] Hao P, Wang B, Du KF, Li G, Tian K, Sun Y, et al. Imperfection-insensitive design of stiffened conical shells based on equivalent multiple perturbation load approach. Compos Struct 2016;136:405–13.
[53] Li., S., Georgiadis, D.G., Kim, D.K., Samuelides, M.S., 2022. A comparison of geometric imperfection models for collapse analysis of ship-type stiffened plated grillages. Engineering Structures, 250, 113480.
[54] Li S, Kim DK, Benson S. The influence of residual stress on the ultimate strength of longitudinally compressed stiffened panels. Ocean Eng 2021;231:108839.
[55] Georgiadis, D., Samuelides, M.S., Li, S., Kim, D.K., Benson, S., 2021. Influence of stochastic geometric imperfection on the ultimate strength of stiffened panel in compression. Developments in the Analysis and Design of Marine Structures: Proceedings of the 8th International Conference on Marine Structures (MARSTRUCT), Trondheim, Norway.
[56] Li, S., Hu, Z., Benson, S., 2020. The sensitivity of ultimate ship hull strength to the structural component load-shortening curve. In Proceeding: The 30th International Ocean and Polar Engineering Conference (ISOPE), Shanghai, China.
[57] Li, S., Benson, S., Dow, R.S., 2021. A Timoshenko beam finite element formulation for thin-walled box girder considering inelastic buckling. Developments in the Analysis and Design of Marine Structures: Proceedings of the 8th International Conference on Marine Structures. Trondheim, Norway.
[58] Kim DK, Ban I, Poh BY, Shin SC. A useful guide of effective mesh-size decision in predicting the ultimate strength of flat- and curved plates in compression. J Ocean Eng Sci 2022. https://doi.org/10.1016/j.joes.2022.02.014. In press.